INVESTIGATION OF BIOLOGICAL AND ORGANIC MOLECULAR ASSEMBLY

A Thesis Submitted to
the Graduate School of Engineering and Sciences of
İzmir Institute of Technology
in Partial Fulfillment of the Requirements for the Degree of

MASTER OF SCIENCE

in Biotechnology

by
Gizem MENDİREK

July 2016
İZMİR

We approve the thesis of **Gizem MENDİREK**

Examining Committee Members:

Assist. Prof. Dr. Hadi M. ZAREİE
Department of Materials Science and Engineering, İzmir Institute of Technology

Assoc. Prof. Dr. Şerafettin DEMİÇ
Department of Metallurgical and Materials Engineering, İzmir Katip Çelebi University

Assist. Prof. Dr. Nur Başak SÜRMELİ
Department of Bioengineering, İzmir Institute of Technology

25 July 2016

Assist. Prof. Dr. Hadi M. ZAREİE
Supervisor, Department of Materials Science
And Engineering, İzmir Institute of Technology

Assist. Prof. Dr. Ufuk ŞENTÜRK
Co-Supervisor, Department of
Materials Science and Engineering,
İzmir Institute of Technology

Assoc. Prof. Dr. Engin ÖZÇİVİCİ
Head of the Department of Biotechnology
and Bioengineering

Prof. Dr. Bilge KARAÇALI
Dean of the Graduate School of
Engineering and Sciences

ACKNOWLEDGEMENT

I would like to thank my supervisor Assist. Prof. Dr. Hadi M. Zareie for his guidance, his endless patience and support. Without his expertise and support, I would have never been able to complete this study.

I would like to express my appreciations to the committee members of my thesis Assist. Prof. Dr. Nur Başak Sürmeli and Assoc. Prof. Dr. Şerafettin Demiç for their participation.

I would like to thank Prof. Dr. Mehmet Sarıkaya, Prof. Dr. Deniz Hür and Dr. Sema Demirci Uzun for letting me use their molecules in this study.

I would like to thank Merve Karakaya and Begüm Yavaş for ellipsometry measurements and Assoc. Prof. Dr. Özgür Birer for XPS measurements.

I would like to give my dearest thanks to all of my friends and colleagues who helped me through my study with their collaborations and gave me motivation with their kind friendships. Thanks for being a second family to me.

Words cannot express my gratitude to my dear parents for their endless love and support. I am grateful to them for always believing in me and for their motivation during my whole life. Thanks for always being there for me.

A special mention goes to my late grandfathers who always believed in me. Although they are no longer with us, they are forever remembered. To them I dedicate this thesis.

ABSTRACT

INVESTIGATION OF BIOLOGICAL AND ORGANIC MOLECULAR ASSEMBLY

Self-assembled monolayers (SAMs) are well-defined and ordered films of molecules that are spontaneously deposited on a surface. By designing molecules with desired head groups for binding specific surfaces, such SAMs can be interesting for a lot of applications such as molecular electronics and biosensors.

In this study, SAMs of organic and biological molecules have been investigated. SAMs of thiophenol, a newly designed Schiff base (E)-4-((4-(phenylethynyl)benzylidene)amino)benzenethiol molecule, a newly designed 4-(4,7-di(thiophen-2-yl)-1H-benzo[d]imidazol-2-yl)benzaldehyde monomer were studied. Mixed SAMs of biotin and streptavidin and graphite binding peptide assemblies are also studied. SAMs were prepared by solution phase method. The gold surface and graphite surface were used as a substrate, because they are both chemically inert to oxidation and flat surfaces. Scanning Tunneling Microscope (STM) was the main experimental technique used here. It was used to obtain images of SAMs at an atomic scale. Scanning Tunneling Spectroscopy (STS) was used to provide information about the local density of states of molecules. Spectroscopic Ellipsometry (SE) was used to measure the monolayer thickness. Contact Angle Measurements was used to determine the surface wettability. X-Ray Photoelectron Spectroscopy (XPS) was used to analyze surface chemistry of SAMs. Surface-Enhanced Raman Spectroscopy (SERS) was used to identify the molecules on a surface.

ÖZET

BİYOLOJİK VE ORGANİK MOLEKÜLER YAPILANMALARIN İNCELENMESİ

Öz-düzenli tek katmanlar yüzeyde kendiliğinden tanımlanmış ve sıralanmış moleküllerden meydana gelen filmlerdir. Belirli yüzeylere bağlanması için istenilen baş gruplara sahip moleküller dizayn edilmesi durumunda, öz-düzenli tek katmanlar moleküler elektronik ve biyosensör gibi birçok uygulama alanı için ilgi çekici olabilir.

Bu çalışmada, biyolojik ve organik moleküllerden meydana gelen öz-düzenli tek katmanlar incelenmiştir. Tiyofenol, yeni dizayn edilmiş Schiff yapılı (E)-4-((4-(feniletilin)benziliden)amino)benzentiyol, ve yeni dizayn edilmiş 4-(4,7-di(tiyofen-2-il)-1H-benzo[d]imidazol-2-yl)benzaldehit molekülleri ile çalışılmıştır. Biyotin ve streptavidin ile karışık öz-düzenli tek katmanlar ve grafite bağlanan peptit yapıları da çalışılmıştır. Öz-düzenli tek katmanlar çözelti fazı metodu ile hazırlanmıştır. Altın ve grafit yüzeyler alttaş olarak kullanılmıştır, çünkü her ikisi de kimyasal olarak oksidasyona karşı etkisiz ve düz yüzeylerdir. Taramalı Tünelleme Mikroskobu kullanılan ana deneysel tekniktir. Öz-düzenli tek katmanların atomik düzeyde görünlenmesinde kullanılmıştır. Taramalı Tünelleme Spektroskopisi moleküllerin lokal yoğunluk düzeyleri hakkında bilgi edinmek için kullanılmıştır. Spektrokopik Ellipsometre tek katman kalınlığını ölçmek için kullanılmıştır. Kontakt açısı ölçer ile yüzey ıslanabilirliği hakkında bilgi edinilmiştir. X-Işını Fotoelektron Spektroskopisi ile öz-düzenli tek katmanların yüzey kimyası analiz edilmiştir. Yüzeyde Güçlendirilmiş Raman Spektroskopisi ile yüzeydeki moleküller tayin edilmiştir.

TABLE OF CONTENTS

LIST OF FIGURES

Figure **Page**

LIST OF ABBREVIATIONS

SAMs	Self-Assembled Monolayers
STM	Scanning Tunneling Microscope
STS	Scanning Tunneling Spectroscopy
XPS	X-Ray Photoelectron Spectroscopy
SERS	Surface-Enhanced Raman Spectroscopy
SE	Spectroscopic Ellipsometry
AFM	Atomic Force Microscopy
UHV	Ultra-High Vacuum
LDOS	Local Density of States
GrBP5	Graphite-Binding Peptide
EPBB	*(E)*-4-((4-(Phenylethynyl)benzylidene)amino)benzenethiol
BIBA	4-(4,7-Di(thiophen-2-yl)-*1H*-benzo[d]imidazol-2-yl)benzaldehyde
HOPG	Highly-Oriented Pyrolytic Graphite
SPIP	Scanning Probe Image Processor

CHAPTER 1

SELF-ASSEMBLED MONOLAYERS

1.1. Concept of Self-Assembled Monolayers

Self-assembled monolayers (SAMs) forms spontaneously on surfaces as two-dimensional ordered layers of molecules with the strong interactions between molecules and surface. SAMs can provide a unique way to control the properties of nanomaterials for the fabrication of nanoscale devices with higher performance. Self-assembly is considered to be an important fabrication technique in nanotechnology.

In 1946, Zisman and his coworkers [1] showed the self-assembly monolayer of a surfactant on a metal surface. His study did not get enough attention, and it led up only a limited level of interest. In the late 1970s Sagiy succeeded to adsorb trichlorosilanes onto silicon oxide [2, 3]. In the early 1980s, Nuzzo and Allara revealed thiols SAMs on gold surfaces by the adsorption of di-n-alkyl disulfides [4]. Their study became the most popular SAM system and drew so much attention on SAMs studies which opened a lot of doors for molecular electronics. Since then, the interest for SAMs has been on the rise and the improvement of surface characterization techniques have resulted as better understanding of monolayer structure and its growth process. Schematic representation of SAMs can be seen in Figure 1.

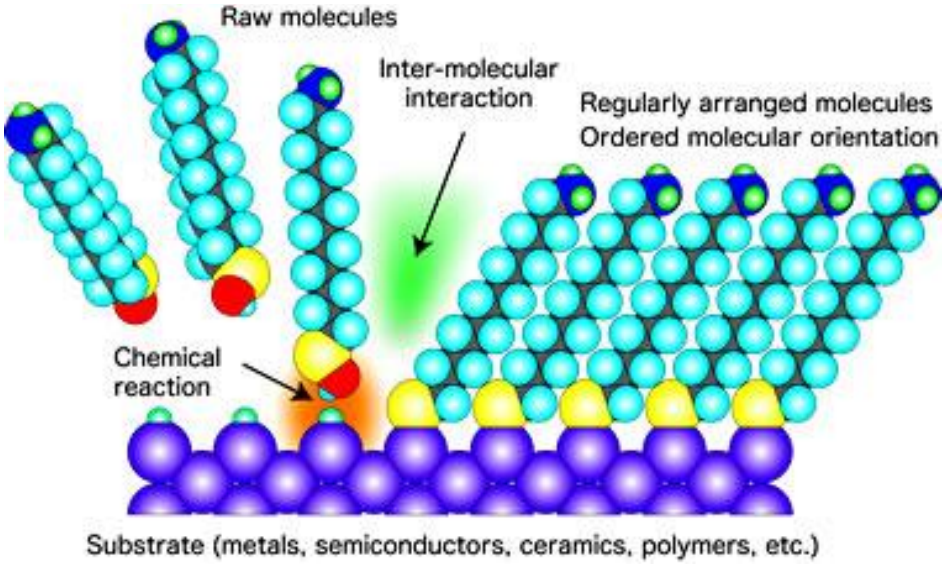

Figure 1. Schematic representation of SAMs.

In principle, SAMs consist of three parts; head group, molecular backbone, and end group as shown in Figure 2(a). Head groups are responsible for specific bindings for surface and they are commonly hydrophilic. They dominate all convenient binding sites on the surface via chemical bonds or non-covalent interactions during the formation of SAMs. Even after the rinsing off of the surface, monolayer formation remains stable. There are a lot of head groups that binds specifically to the surfaces for SAMs formation, e.g. thiols or disulfides on gold, silanes on SiO_2, phosphates for metal oxides [5, 6], fatty acids for aluminum oxide [7] and silver [8], isonitriles for platinum [9]. Molecular backbones connect the head group and end group of a molecule. The most studied molecular backbones are alkyl groups. Their role for the formation of ordered and closely packed SAMs via van der Waals interactions up to a order of few (<10) kcal/mol is really significant for SAMs systems [10]. Phenyl rings have a π system, and in that case π-π interactions should be considered. The strength of these kind of intermolecular interactions are the reason for the spacing that occurs between the head groups [11]. It also affects the interface properties of the system.

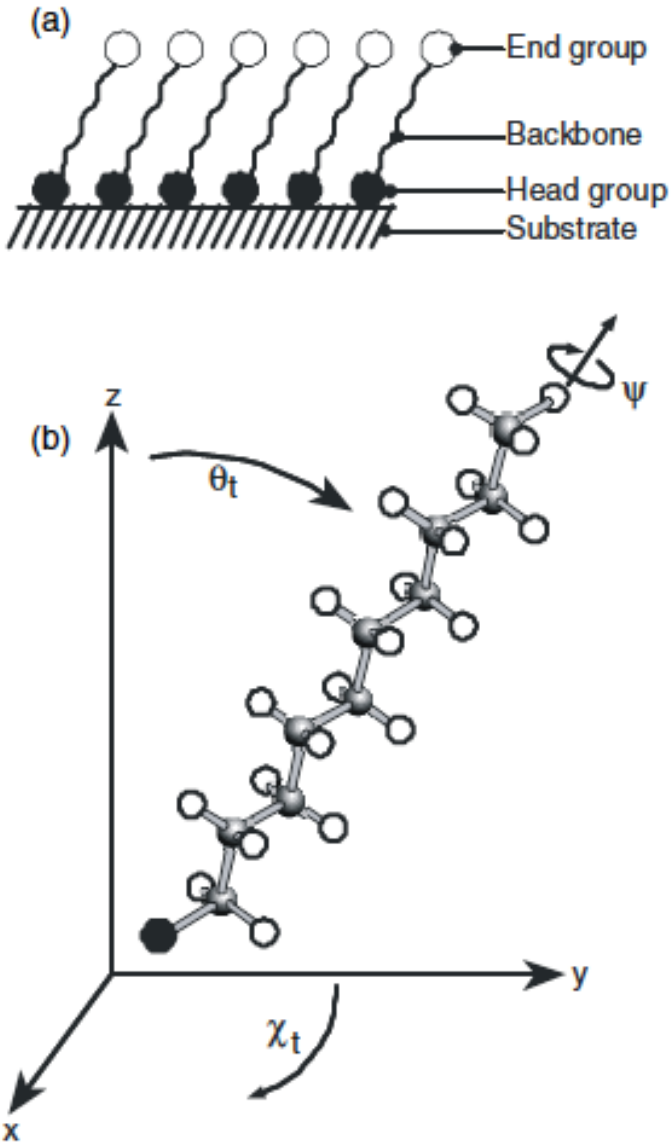

Figure 2. (a) Schematic representation of three parts of SAMs; head group, backbone, end group. (b) Schematic representation of three parameters of SAMs; tilt angle (θ_t), twist direction (χ_t) and twist angle (ψ) [12].

There are three different parameters that can describe the structure of the molecular backbone in a SAM system as shown in Figure 2(b). First parameter is the tilt angle (θ_t) which is the angle between the surface normal, second parameter is the tilt direction (χ_t) which is the projection of molecule in the x-y plane, and the last parameter is the twist angle (ψ) which is the angle of rotation around the molecule axis. End group represents the outer part of the molecule that points away from the substrate. In a SAM system, they provide a possibility for a change in the interface between the molecule and the substrate. The change in the terminal groups can be resulted in different

properties in SAMs. For example, SAMs with an end group of –COOH, –OH and $-NH_2$ are hydrophilic, with an end group of $-CH_3$ are hydrophobic, with an end group of $-CF_3$ have a strong dipole at the surface [13].

Characterization techniques are needed in order to understand the surface properties. There are various characterization techniques for studying SAM systems such as ellipsometry, surface plasmon resonance spectroscopy (SPR), infrared reflection absorption spectroscopy (IRRAS), X-ray photoelectron spectroscopy (XPS), contact angle measurements, atomic force microscopy (AFM) and scanning tunneling microscopy (STM) [14, 15]. All these techniques provide information about thickness, wettability, functional groups, structure and etc.

1.2. Preparation methods of Self-Assembled Monolayers

In general, there are two ways for the development of SAMs; solution phase and vapor phase methods. The most common method is the solution phase, which can be easily prepared by immersing the substrate into a solution for a desired period of time. The usage of solution phase method is advantageous because it is easy to prepare the monolayers as shown in Figure 3. However, there are some disadvantages of this method and these are mostly about not being able to be fully informed about the growth process of SAMs, because solution phase method is not consistent with in-situ techniques that are used to obtain information about the growth process. Furthermore, there are different factors, which affects the solution phase such as temperature, concentration, structure of molecules and choice of solvent [16]. For example, lower molecular concentration may need more immersion time for less defects on the SAMs. Another example can be given about carboxylic acid terminated SAMs. There is repulsion between the carboxylate groups and as reports stated their SAMs resulted in unstructured monolayers because of this repulsion [17]. Therefore, during the preparation of monolayers acidifying of the solution is needed [18]. Cleanliness of the substrate is also another factor since it affects the growth behavior and the quality of the monolayers.

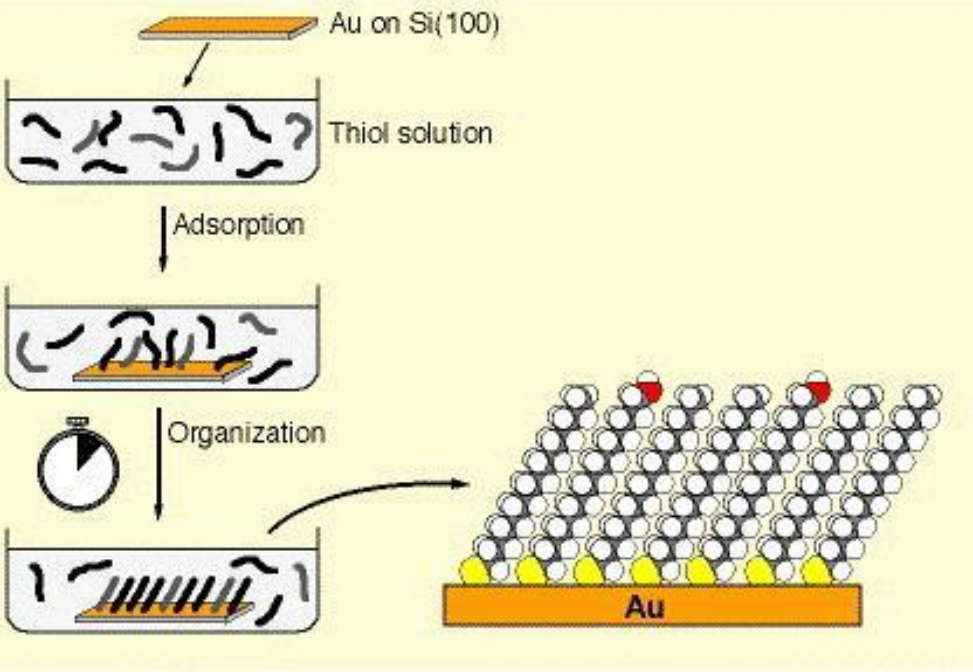

Figure 3. Preparation of SAMs by solution phase method.

The second method for the deposition of SAMs is the vapor phase. In the vapor phase method, molecules adsorb onto the substrates by evaporating the molecules in a UHV chamber or in a desiccator as shown in Figure 4. There are more experimental process in the deposition of molecules via vapor phase method compared to the deposition of molecules via solution phase method. Vapor phase method has many advantages over solution phase method. These advantages can be listed as controlling the cleanliness of substrate and the variety of compatible experimental techniques for using in UHV chamber which is useful for investigating the growth process of SAM formation [19]. It may also have an advantage during the preparation of SAMs in real-time characterization.

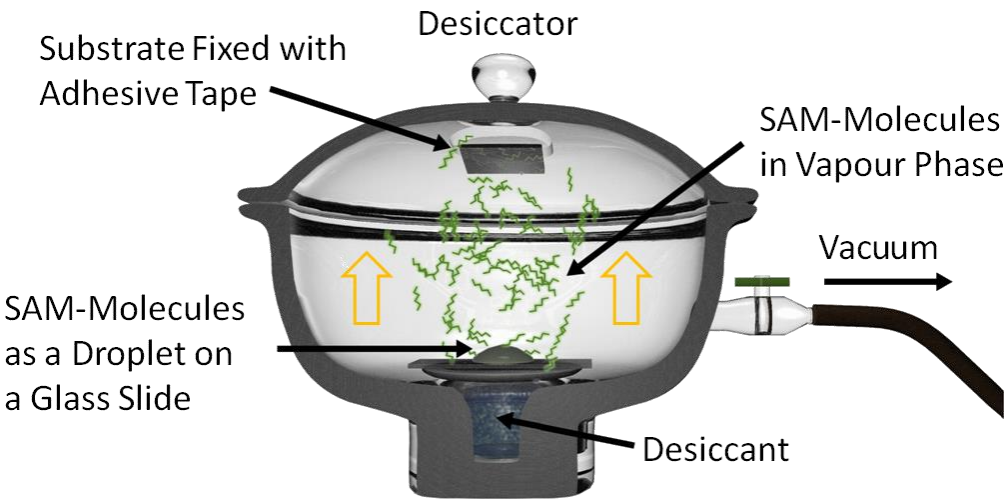

Figure 4. Preparation of SAMs by vapor phase method [20].

1.3. Self-Assembled Monolayers Kinetics and Growth Mechanism

Designation of SAMs is related to the self-assembly process, hence it is important to understand this process well. The well-known SAMs system is known to be SAMs of alkanethiols on gold [21, 22]. The growth of the molecular monolayer can be explained with Langmuir growth curve [23]. It goes exponentially until the coverage saturation occurs. Further studies showed that there are different phases in the growth process, which can be grouped in two stages.

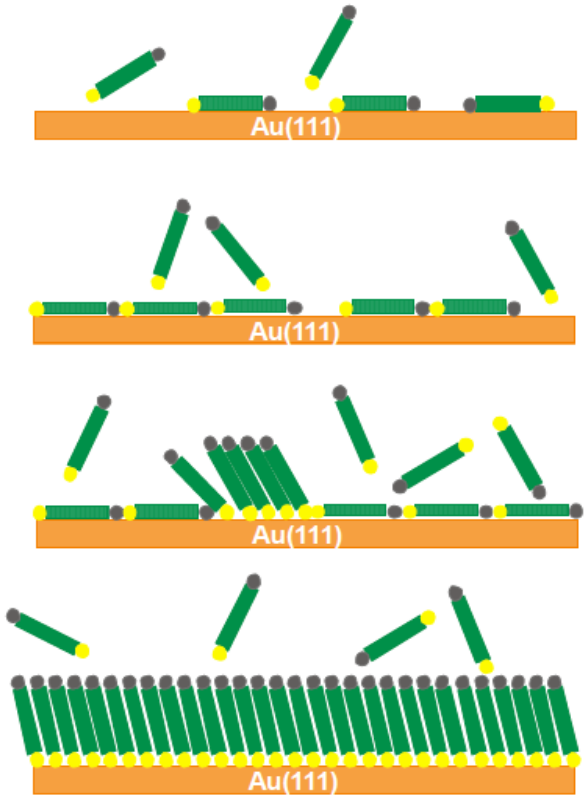

Figure 5. Formation of SAMs showing striped phase and stand-up phases.

In the first stage, adsorption of molecules and formation of the bonds between head group and the surface occur in the first few minutes of the growth process. Studies showed that molecular adsorption can covered the %80 of the surface successfully in the first stage of the growth process [16]. Yamada [24] and Sylvain [25] showed that the ordered assemblies of the alkanethiols in the first stage of growth process by using an in-situ scanning probe microscopy. They observed that the molecules lying flat on which is also called as ‘’striped phase’’. SAMs prepared with vapor phase method mentioned above was observed too and the same structure was revealed with lower surface coverage. Increase in surface coverage results in formation of islands at the domain boundaries. Lateral pressure causes molecules to form a standing-up position at the surface and as a result, these islands are formed [26].

In the second stage, molecular organization takes place until they reach their equilibrium and form an ordered monolayer. It takes several hours to reach the equilibrium, in other words, second stage of growth process lasts several hours [10]. It is also called as ‘’stand-up phase’’. Intermolecular interactions, such as van der Waals

interaction, are the reason of molecular organization on the surface. The final structure of the SAMs as shown in Figure 5 includes both head group – surface interaction which occurs at the first stage and the intermolecular interaction at the second stage of growth process.

1.4. Applications of Self-Assembled Monolayers

Self-assembled monolayers have been a hot topic and studied in recent years for a variety of applications. Since SAMs provide surface modification, applications of SAMs can expand to a variety of fields (Figure 6) such as molecular electronics, biosensors, lithography patterning, drug delivery and lubrication [27-29].

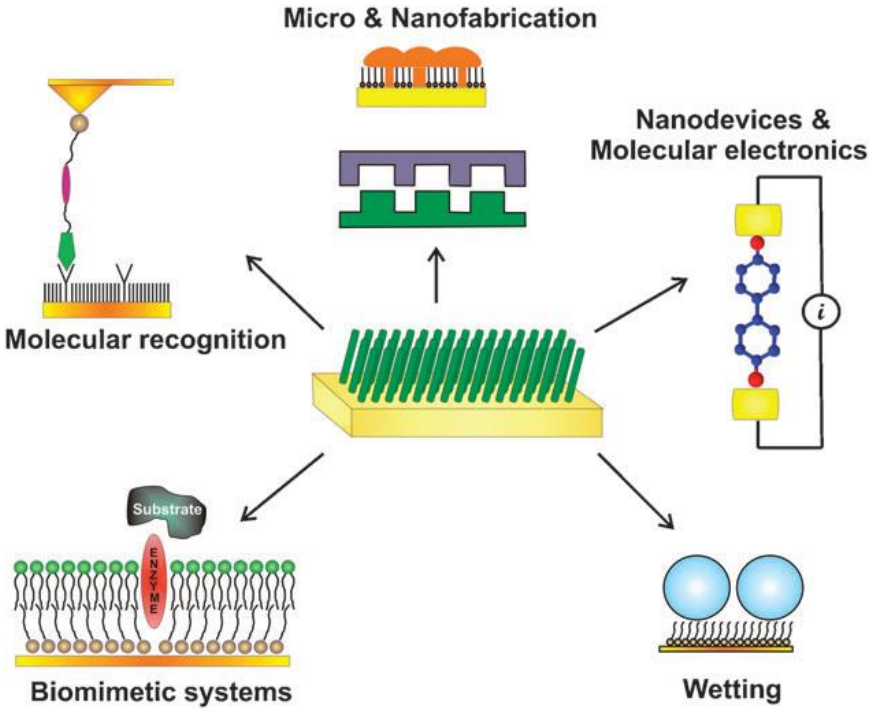

Figure 6. Some applications of SAMs [30].

Densely packed and stable SAMs can prevent substrates from corrosion and wear [31]. Furthermore, some properties of SAMs such as composition and structure, allow them to be used in sensor applications [32]. SAMs are favorable factor for optoelectronic devices [33]. Moreover, SAMs are beneficial for different conformations that depends on orientations of the end groups [34].

1.5 Mixed Self-Assembled Monolayers

When a mixture of different molecules adsorbed on the surface forms a monolayer, it is called as mixed self-assembled monolayer (mixed SAM). Surface properties can be controlled by the co-adsorption of molecules that have different functional groups. It also leads to the control of chemical functionalities. Mixed SAMs can improve the quality of the monolayer by preventing steric hindrance between molecules during the formation of monolayers. Mixed SAMs as shown in Figure 7 usually prepared by a mole fraction ratio of different molecules that binds on the surface and this ratio in solution is often not the same as the ratio on the surface. It depends on the molecular structure, chain length and different end groups of molecules [35-37].

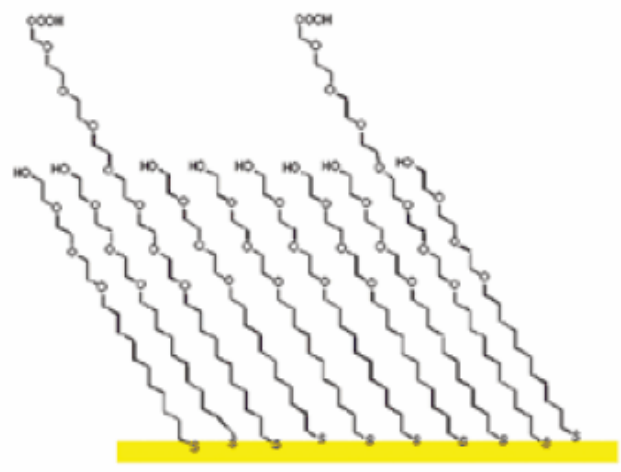

Figure 7. Monothiol mixed SAMs.

Co-adsorption of molecules at elevated temperatures is a way to form ordered mixed SAMs and it results in well-ordered SAMs with molecules of different end groups and chain lengths. Some factors affect the final adsorption states of SAMs such as concentration, temperature and immersion time. These factors have an impact on defect sizes and can be used to control the quality of mixed SAMs. Formation of mixed SAMs can be considered as a favorable design to study properties of a single molecule.

CHAPTER 2

CHARACTERIZATION TECHNIQUES

2.1. Contract Angle Measurements

Contact angle measurement is an important technique to get surface information such as wettability, adhesion properties and surface tension of solid surfaces. When a liquid drop is applied to a solid surface, the angle between the tangent of the liquid drop and the surface is called contact angle (θ), which is related to surface tension and can be calculated via Young's equation [38].

$$\gamma SV = \gamma SL + \gamma LV \cos\theta \qquad \text{(Equation 1)}$$

where, θ is the contact angle and γLV, γSV and γSL are the liquid-vapor, solid-vapor and solid-liquid surface tensions respectively as shown in Figure 8. These are three interfacial forces that the liquid drop is under at mechanical equilibrium. Surface tension is basically what determines the shape of the liquid drop. Water is the most commonly used liquid for contact angle (θ) measurements. Water spreads over the surface if the contact angle is smaller than 90 degrees and it is called hydrophilic surface. If the contact angle higher than 90 degrees, water beads up on the surface and it is called hydrophobic surface.

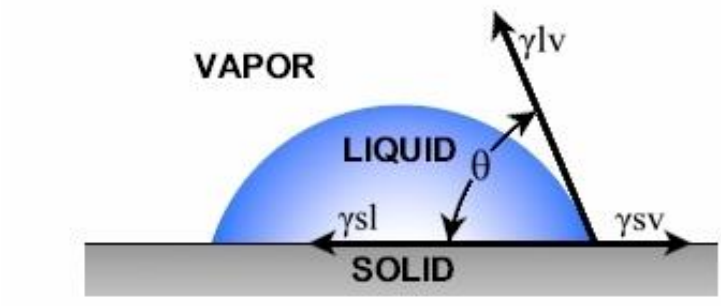

Figure 8. Schematic representation of a liquid drop showing the contact angle and Young's Equation variables.

There are two modes of contact angle measurements that can be performed. In static mode, the volume of the liquid drop remains constant and the contact angle is measured as the average of the angles on the right and left side of the sessile drop. On the other hand, in dynamic mode, the volume of the liquid drop is changed by expanding and contracting the liquid which forms advancing contact angle θa and receding contact angle θr. The difference between the advancing angle and the receding angle is called hysteresis. Hysteresis can give information about surface roughness and heterogeneity [39]. In general, contact angle measurements can be used to determine whether a thin film is properly coated on the substrate or to obtain indications of the organization of SAMs on the surface and the effects of the surface energy on the adsorption process.

2.2. X-Ray Photoelectron Spectroscopy (XPS)

X-ray Photoelectron Spctroscopy (XPS), also known as Electron Spectroscopy for Chemical Analysis (ESCA), is a powerful surface analysis technique that provides information about the elemental composition of surfaces and chemical environment of an atom at the surface [40]. XPS was invented by K. Siegbahn and his co-workers in mid 1960s [41]. It is based on the photoelectric effect, which was discovered by Heinrich Hertz in 1887 [42] and explained by Albert Einstein in 1905 [43]. Photoelectric effect basically refers to the emission of electrons from a surface when the surface is irradiated with incident photon. Kinetic energy (KE) of the emitted electrons are;

$$KE = h\nu - E - \varphi \qquad \text{(Equation 2)}$$

where E is the binding energy of the electron and φ is the work function of the material. The binding energy is determined by the difference between the energy of the incident photon and the kinetic energy of the emitted electron [44]. XPS consists of a source of energy to emit X-rays and an electron energy analyzer to measure the kinetic energy of emitted electrons.

To study the properties of core electrons of the atom high energy X-rays are essential. Most widely used sources to obtain X-ray in XPS are Al (1486 eV) and Mg

(1253 eV) [45]. Basically, an XPS spectrum is obtained by irradiating a source with a beam of X-rays while measuring the kinetic energy (KE) and number of electrons that are emitted from the surface at the same time. XPS can be used to determine the composition of the sample. The measurement of kinetic energies enables elemental analysis because two elements do not share the same set of electronic binding energies. In other words, each element develops a set of XPS peaks at characteristic binding energies that directly classify each element that is present in the surface. These characteristic peaks correspond to the electron configuration of the electrons within the atoms, e.g., 1s, 2s, 2p, 3s, etc. The total number of the element within the area irradiated is associated with the number of detected electrons in the characteristic peaks [46]. XPS also enables the determination of the composition quantitatively with the help of peaks heights. The changes in the chemical environment can be tracked down by monitoring the changes in their photoelectron energies, which can be seen as small shifts in the peaks in the XPS spectra, so-called chemical shifts.

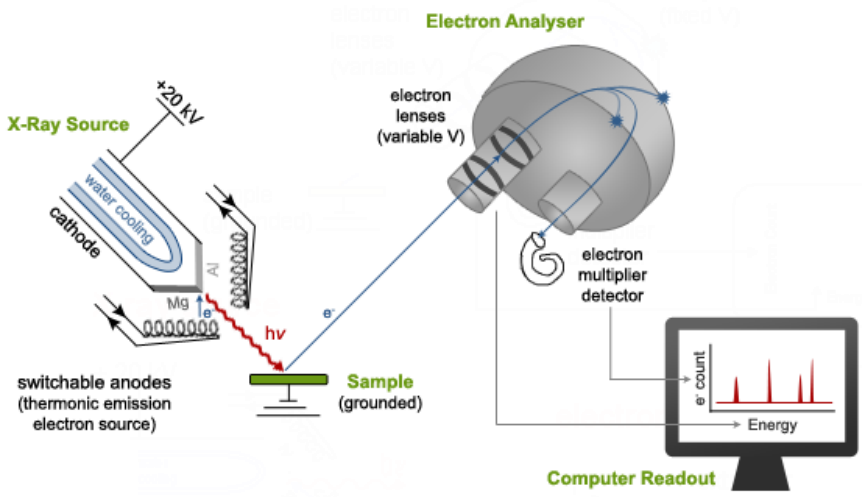

Figure 9. Schematic diagram of X-ray Photoelectron Spectrometer.

XPS measurements must be performed under ultra-high vacuum (UHV) environment. The detectors that count electrons in the XPS apparatus (Figure 9) work with the minimum error in UHV. This technique is considered to be destructive because there is a lot of loss of material from the sample. Hence, a sample analyzed by XPS will not be able to be analyzed by other techniques. Surface sensitivity of XPS, which is approximately 5 nm, is a result of the short electron mean-free-path in a solid [47].

2.3. Ellipsometry

Ellipsometry is an optical characterization technique that is used to measure optical properties and thickness of thin films. It is a non-destructive method and based on the change in polarization reflected from the surface, expressed as Ψ (amplitude ratio) and Δ (phase difference). Ψ and Δ are also called as ellipsometric angles [48]. When a polarized light reflects from a sample surface, it decomposes as s-polarized and p-polarized components which represents the perpendicular and parallel components to the plane of incidence of reflected light, respectively as shown in Figure 10. The amplitudes of these two components after reflection are denoted as Rs and Rp, respectively. The basic equation in ellipsometry is as follows:

$$\rho = \frac{Rp}{Rs} = \tan(\Psi)e^{i\Delta} \qquad \text{(Equation 2)}$$

Where ρ is the complex ratio between the Fresnel coefficients of light (s-polarized and p-polarized components respectively), tanΨ is the amplitude change upon reflection, and Δ is the phase shift. Since the only measured values by ellipsometry are Ψ and Δ, they are not very helpful to obtain surface properties by themselves.

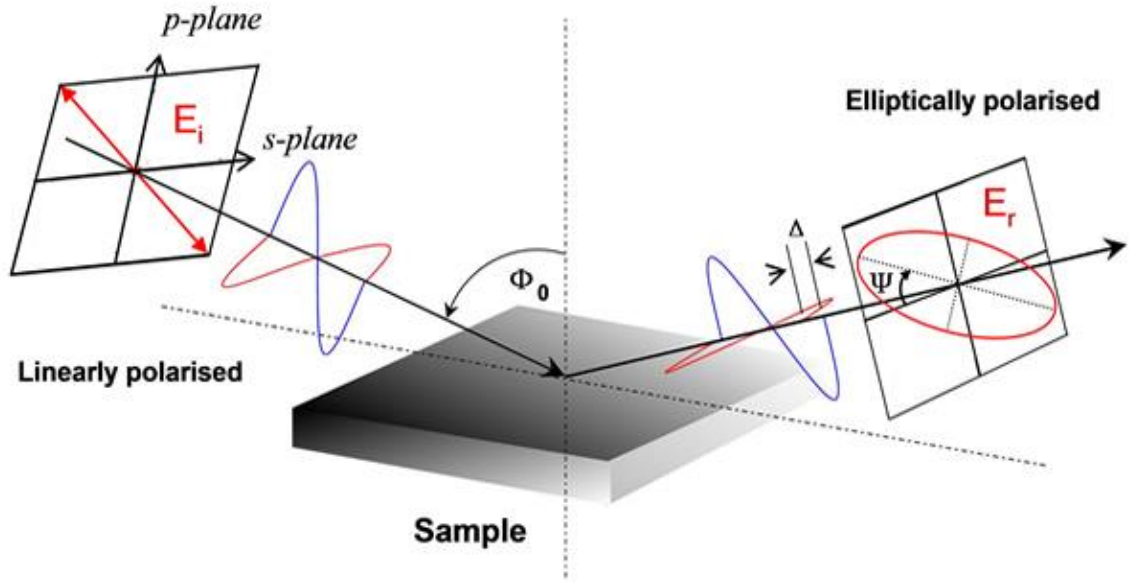

Figure 10. Schematic overview of an ellipsometric measurement.

To associate these measured values with surface properties, some theoretical models are needed. It is possible to obtain surface properties of the sample, such as refractive index and thickness of the sample by fitting the measured values (Ψ and Δ) to the desired models. For example, three-phase model [49] is usually used to determine thin film thickness. This model consists of an ambient/thin film/substrate structure and refractive indexes have to be known for all three media. Another model called as Forouhi - Bloomer model [50] is used to determine optical constants of the sample, such as refractive index, n, and extinction coefficient, k. In addition to film thickness and optical constants of the sample, ellipsometry measurements can also provide information about surface roughness, interfacial layers, and anisotropy.

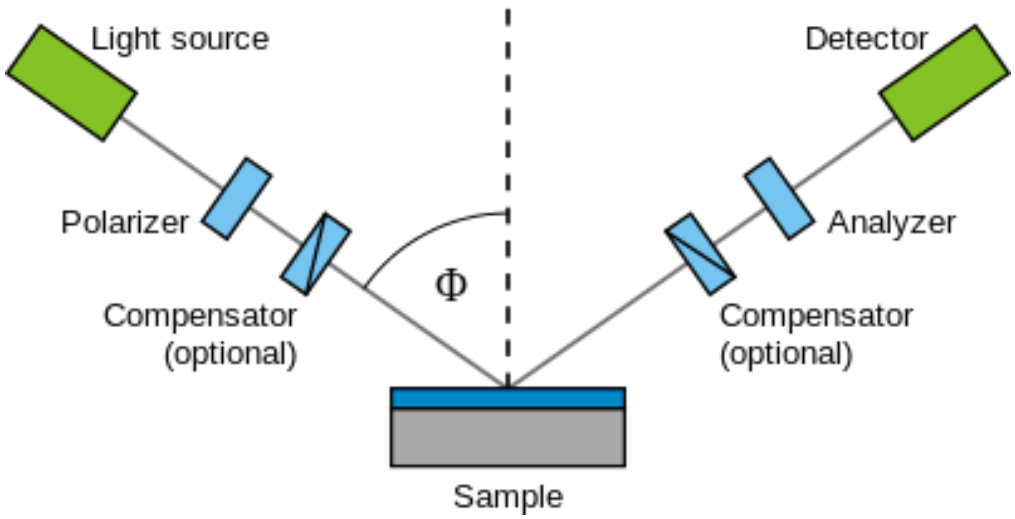

Figure 11. Components of ellipsometry.

The primary tools to have for data acquision in an ellipsometer are that light source, polarizer, analyzer and detector as shown in Figure 11. Light is linearly polarized by the polarizer and reflects from the surface, results in a change of polarization state. After reflection, it passes through the analyzer and lastly the detector to finish its optical path.

2.4. Scanning Tunneling Microscope and Spectroscopy (STM/STS)

Scanning tunneling microscope (STM) is a powerful technique for surface analysis with three-dimensional, real-time imaging at atomic scale. It was invented in 1982 by Binning, Rohrer and co-workers who were later awarded for Nobel Prize in Physics in 1986 [51]. The resolution of STM is considered to be good as it has 0.1 nm lateral resolution and 0.01 nm depth resolution [52]. The concept of STM is based on quantum mechanical tunneling. When two conductors are brought close to each other and separated by a potential barrier, due to the overlapping wave functions of electrons in the conductors, electrons can tunnel through the barrier between these two conductors. To operate the STM, a very sharp conducting tip is brought close to a conductive or a semi-conductive surface and when a small voltage is applied between the tip and the surface, it generates a tunneling current of electrons tunneling from tip to surface, or vice versa, depending on the sign of the bias voltage applied. Measuring the tunneling current between the tip and the surface leads to produce the topographic images of the surface. Tunneling current varies with the distance between the tip and the surface. The motion of the tip is provided with a piezoelectric material, which can be controlled by a computer by changing the voltage that is applied to it as shown in Figure 12. During the scanning process, the computer controls this piezoelectric material to raster scan the tip over the surface and the resolution of a STM image is dependent on the sharpness of the tip.

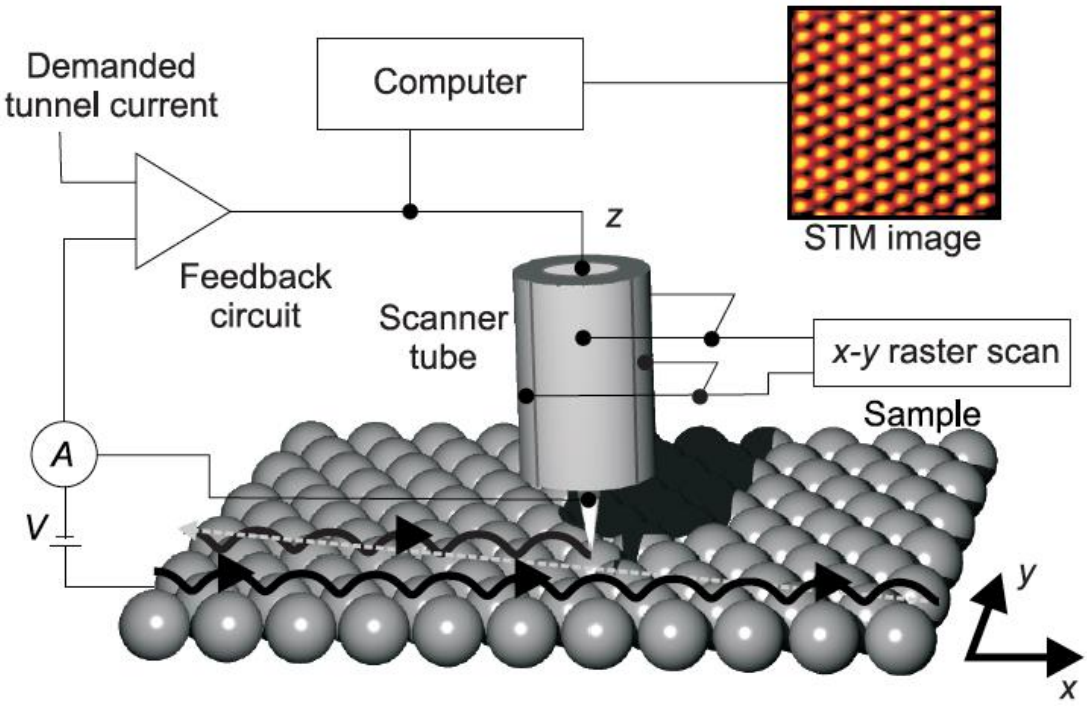

Figure 12. Components of STM.

There are two modes of STM that can be operated with;

In constant current mode, a feedback system keeps the tunneling current constant by adjusting the separation between the tip and the sample surface as shown in Figure 13(b). In other words, if there is an increase in the tunneling current, the feedback system adjusts the voltage that has to be applied and it causes the tip height to change until the tunneling current becomes constant again. The change of the tip height is recorded as a function of position by computer and displayed as an STM image.

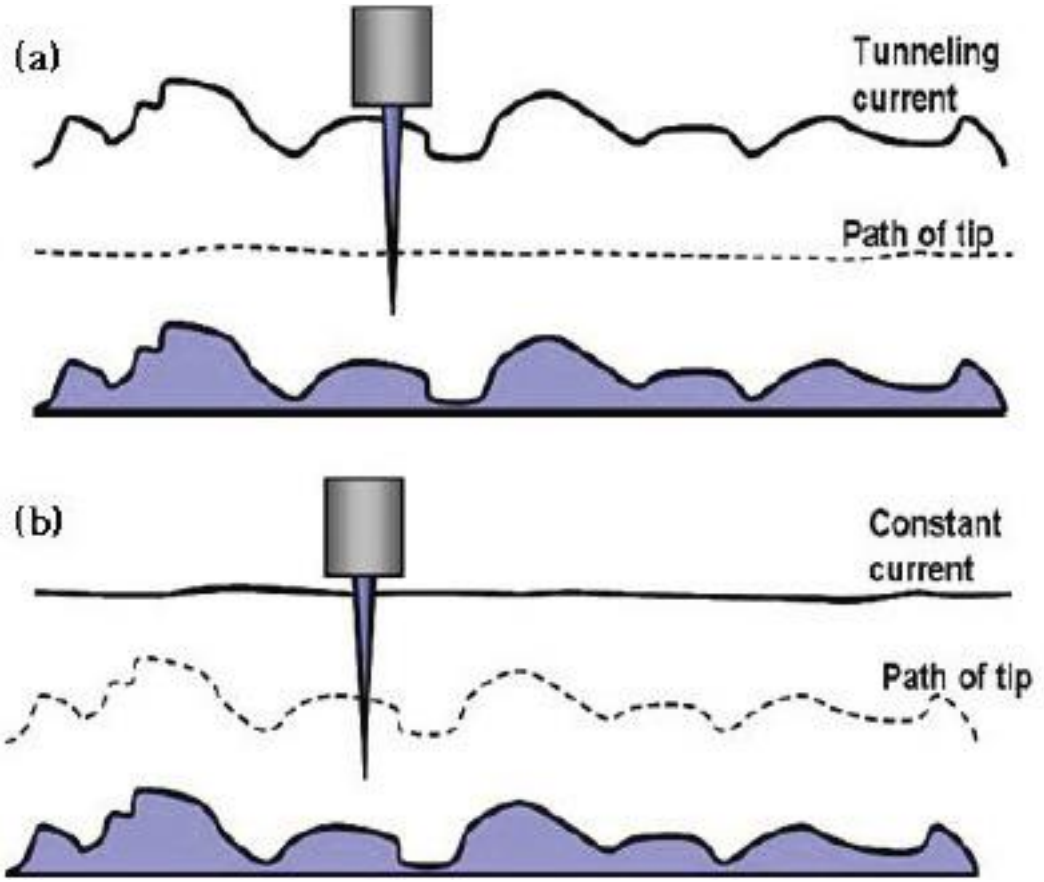

Figure 13. Schematic representation of (a) constant-height (b) constant-current mode of STM.

In constant height mode, the tip scans over the surface at a fixed line as shown in Figure 13(a). In other words, the tip height is kept constant during the scanning process. Topographic changes over the surface or tip-sample separations causes a change in tunneling current. These changes in tunneling current are recorded to form an STM image. Constant height mode is preferred while scanning atomically flat surfaces since the tip scans at a fixed level and can be crashed during the scanning if the surface is rough. Also, in constant height mode, the scanning process is faster, because the tip does not have to move up and down. On the other hand, while operating with constant current mode, the surface does not necessarily have to be atomically flat.

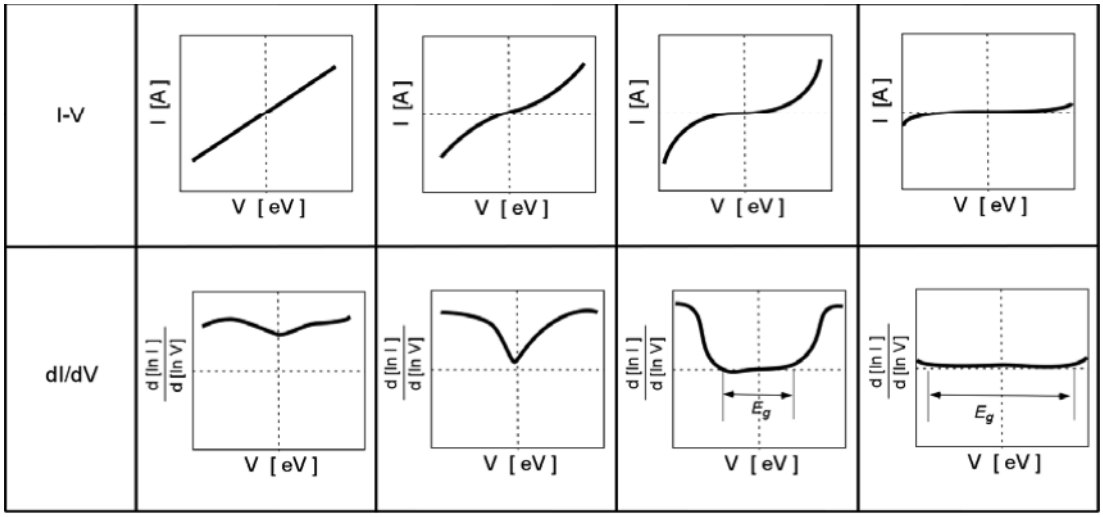

Figure 14. I-V and dI/dV curves of metals, semi-metals, semiconductors and insulators, respectively.

Scanning tunneling spectroscopy (STS) is an extension of STM to study the electronic properties of materials such as local density of states (LDOS) and band gap of surfaces. STS can be performed in two modes: current – voltage (I-V) and current – distance (I-z). In the current – voltage mode, the feedback loop is disabled at a height of fixed tip on surface and the tunneling current is recorded as a function of bias voltage. I-V curves and dI/dV curves of metals, semi-metals, semiconductors and insulators can be seen in Figure 14. Obtained I-V curves provide the band gap of semiconductors. In other words, the energy difference between highest occupied molecular orbital (HOMO) and lowest unoccupied molecular orbital (LUMO) energies of molecules refer to the band gap. In the current – distance mode, again the feedback loop is disabled, but this time the bias voltage is fixed and the tunneling current is recorded as a function of tip-sample distance. I-z curves provide the local barrier heights of samples.

2.5. Surface-Enhanced Raman Spectroscopy (SERS)

SERS was first discovered in 1974 when Fleishman and co-workers discovered that Raman signal for pyridine molecules adsorbed on anodized silver electrodes was greater than expected by a magnitude of at least 10^6, that later on explained by Fleishman as a result of scattering molecules from the surface [53]. In 1977, Van Duyne and co-workers explained the increase in Raman signal with electromagnetic enhancement mechanism (EM) [54]. Later, Albrecht and Creighton introduced a new theory called chemical mechanism (CE) about SERS phenomena that was due to a charge-transfer effect [55]. There are some other theories to explain the mechanism behind the SERS but electromagnetic and chemical mechanisms are the most accepted ones that describe the enhancement effect of SERS.

Electromagnetic mechanism is related to localized surface plasmon resonance (LSPR). Surface plasmon is the oscillating electrons that are at the interface of a material. Localized surface plasmon resonance can be defined as the excitation of surface plasmons by an indicent light as shown in Figure 15. If the surface is smooth, then this excitation energy will be lost. On the other hand, if the surface is considered to be rough, there will be a radiation. If the wavelength of the incident light is in resonance with the LSPR of the surface, there will be an electromagnetic field produced which is the reason of the enhancement for the Raman signal. Electromagnetic mechanism is usually dependent on dielectric properties and roughness of the substrate.

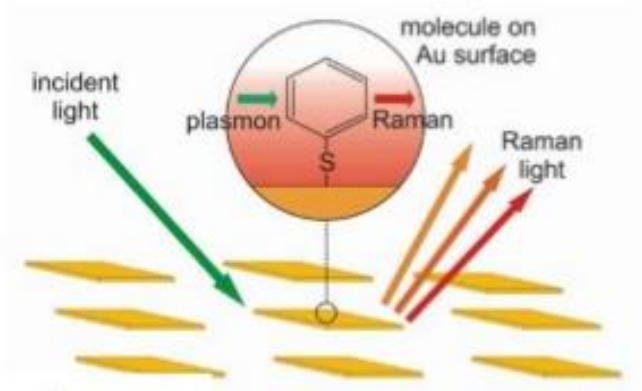

Figure 15. Schematic representation of SERS.

Chemical mechanism is due to a charge-transfer between the adsorbate and the substrate. It is only valid for molecules that are chemically adsorbed on the substrate. When an electron is excited from the substrate into an adsorbed molecule, a negatively charged excited molecule is created by the incident photon. Due to this charge transfer, a relaxation is induced in the newly created excited molecule and this relaxation causes the electron return to the substrate and creates new excited states. Chemical mechanism is dependent on the nature of the molecule and the adsorption sites of the substrate.

Enhancement factor of chemical mechanism is on the order of 10 to 100. On the other hand, enhancement factor of electromagnetic mechanism is on the order of 10^5 to 10^6 [56]. For some systems, the enhancement factor can be as high as 10^{14}, and it means that SERS can be listed as a technique that can detect a single molecule [57, 58].

CHAPTER 3

EXPERIMENTAL

3.1. Materials

Au(111) films on mica were purchased from Phasis, Switzerland. The STM tip was prepared from Pt/Ir wire cut under ambient conditions. All chemicals were used as received. Chloroform (>99%, Merck), ethanol (>99%, Sigma Aldrich), Dichloromethane (>99%, Sigma Aldrich), EZ-Link HPDP-Biotin (Thermo Scientific), Streptavidin from *Streptomyces avidinii* (Sigma Aldrich), thiophenol (>99%, Sigma Aldrich), Phosphate buffered saline tablet (Sigma Aldrich).

3.2. Methods

3.2.1. Sample Preparation

3.2.1.1. Sample Preparation of Organic Self-Assembled Monolayers

Thiophenol (Figure 16(c)) monolayers (SAMs) were prepared by immersing Au(111) into a 1mM thiophenol solution in ethanol at room temperature for 24 hours. The samples were then removed from the solution and washed thoroughly with ethanol and dried using a stream of N_2 gas.

EPBB (Figure 16(a)) was synthesized by Prof. Dr. Deniz Hür at the Department of Chemistry, Anadolu University. EPBB monolayers were prepared by immersing Au(111) in 2-3 ml of solutions of EPBB dissolved in chloroform or dichloromethane (0.1 mM - 1mM) under an argon atmosphere. The samples were kept at room temperature between 16 and 72 hours, then removed from the solution and washed thoroughly with solvent and dried using a stream of N_2 gas.

BIBA (Figure 16(b)) was synthesized by Dr. Sema Demirci Uzun at the Department of Polymer Science and Technology, Middle East Technical University. BIBA monolayers were prepared both on Au(111) and on HOPG substrates. For samples on Au(111) the same solution deposition method that mentioned above used. Au(111) was immersed in BIBA solution (0.1 mM - 1mM) in chloroform at room temperature for various hours, then removed from the solution and washed thoroughly with chloroform and dried using a stream of N_2 gas. To prepare BIBA monolayer on HOPG substrate, a drop of BIBA solution (0.1 mM - 1mM) was deposited on a freshly cleaved HOPG substrate and then dried in a closed environment.

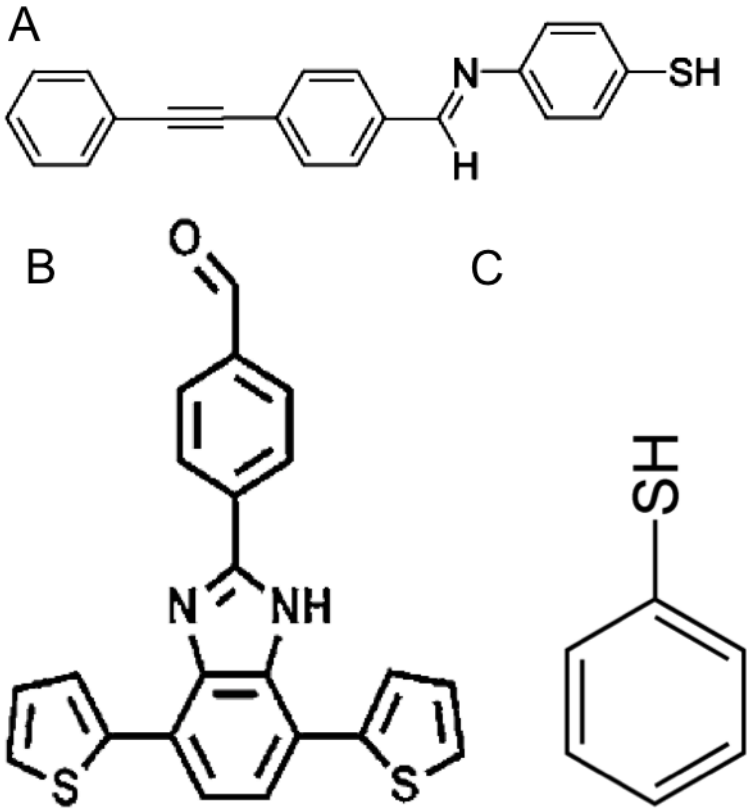

Figure 16. Studied organic molecules. (a) EPBB, (b) BIBA, (c) thiophenol.

All containers used in monolayer formation were heated (70°C) for 30 minutes in a mixture of H2O/H2O2/NH_4OH (5:1:1), then rinsed with water and dried with nitrogen. They were stored in the oven at 60 C until use.

3.2.1.2. Sample Preparation of Biological Self-Assembled Monolayers

A Biotin-HPDP (Figure 17(a)) solution was prepared by dissolving 1 mg of biotin-HPDP in 100 µL of DMF by sonicating at 45ºC, then added to 2 ml of (1:1) water and ethanol mixture. Au(111) was immersed in the biotin-HPDP/thiophenol mixed solution in ethanol at room temperature for 24 hours. The samples were then washed with pure ethanol and dried with nitrogen. Thiophenol molecules were used as spacers in order to make the immobilization of streptavidin molecules easier (Figure 17(b)). Mixed SAM samples were immersed into a 2 µM solution of streptavidin in PBS buffer for three hours, then rinsed with pure water.

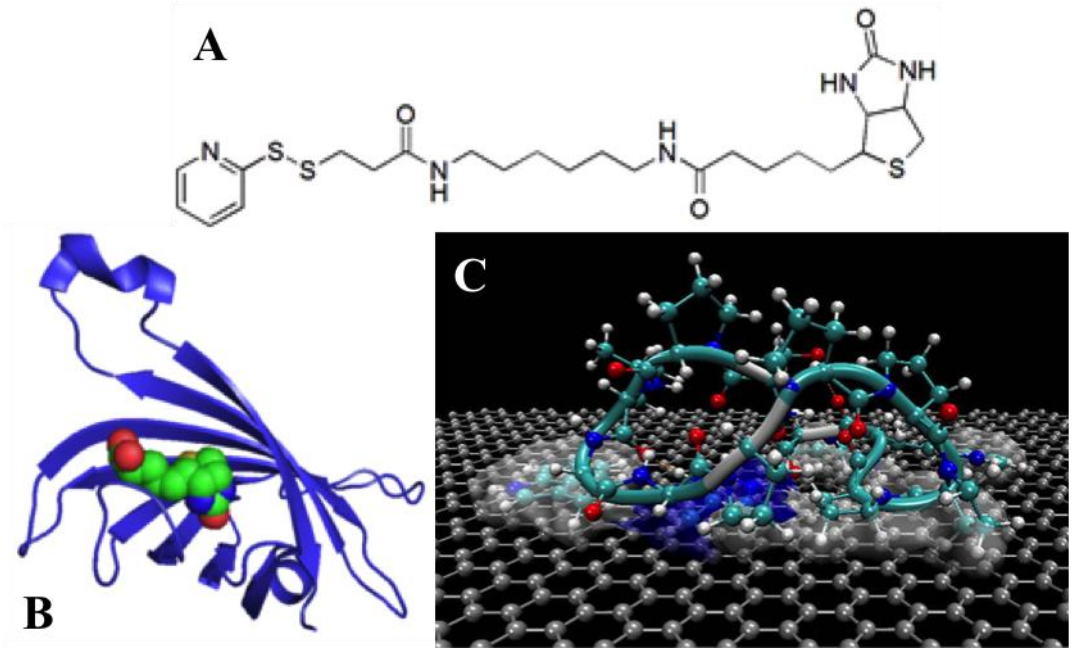

Figure 17. Studied biological molecules. (a) Biotin-HPDP, (b) streptavidin, (c) GrBP5.

GrBP5 (IMVTESSDYSSY) (Figure 17(c)) was designated as the wild-type (WT) peptide at the Department of Materials Science and Engineering, University of Washington. GrBP5 monolayers were prepared by incubating with 2 µM peptide solution in distilled water for 1 hour, then rinsed with water and dried using a stream of N_2 gas.

3.2.2. Characterization Methods

X-Ray Photoelectron Spectroscopy (XPS): Photoemission spectra were recorded with a Thermo Scientific K-Alpha XPS spectrometer furnished with monochromatized Al-Kα x-ray source. Freshly prepared samples of molecular structures on Au(111) were attached to the sample holder with conductive carbon adhesive tape from the back-side. A flood gun, source of low energy charged particles (é, Ar^+), was used for charge compensation during the measurements. The base pressure of the vacuum chamber rose from 2.0×10^{-9} mbar to 2.0×10^{-7} mbar during the measurements. The x-ray spot size was approximately 400 μm. The spectra were recorded with a pass energy of 50 eV, which corresponds to a spectral resolution of ca. 0.5 eV. The spectra were referenced to C1s binding energy at 284.8 eV. The spectral fitting was performed with Avantage v5 software.

Scanning Tunneling Microscopy (STM) and Spectroscopy: STM images were acquired using a Nanosurf EasyScan system under ambient conditions. STM piezoelectric scanners were calibrated laterally, with graphite and Au(111), and vertically, using the height of the Au(111) steps (2.2Å). The STM tip was prepared from Pt/Ir (90%/10%) 0.25-0.2 mm wire cut under ambient conditions. All images were acquired in a constant-current mode. Typical imaging conditions are bias voltage of 200 mV- 1 V and a tunneling current of 50 pA to 1.2 nA. Images shown are raw data unless stated otherwise. Images were manipulated with Scanning Probe Image Processor (SPIP) software. Contrast-enhanced images were obtained by applying a correlation averaging procedure to analyze repeat molecular units and by applying a low-pass filter.

Ellipsometry and Contact Angle: The thickness of the deposited layer on gold was measured by a spectroscopic ellipsometry (M-2000, J.A. Woollam). Spectroscopic data were obtained over a spectral range from 245 nm to 1000 nm with an incident angle of 65º. Refractive indexes of the samples were determined by using a refractometer. A Cauchy layer model was used to fit the data set. Water contact angles were measured on freshly prepared surfaces with an Attension Theta optical tensiometer by Biolin

Scientific. All the reported values are the average of contact angles at 5 different spots per sample

Surface Enhanced Raman Spectroscopy: Raman spectrometer XploRA (Horiba) equipped with a confocal microscope was used. The Raman signals were recorded in a spectral range of 600–2500 cm^{-1} using a 785nm laser excitation, in combination with a 40X objective magnification (NA= 0.65) of an Olympus BX41 transmission and reflection illumination microscope (Olympus, France) for focus and collection of Raman-scattered light. EPBB molecule was dissolved in chloroform (1 mM) and dropped onto SERS plate (S. T. Japan Inc.). In order to investigate the trans-cis transition, the substrate which was dropped onto EPBB solution was irradiated by UV light at 365 nm and then the substrate was heated to 55 °C to induce the transition from cis to trans [45]. For each sample, the Raman experiment was repeated 5 times to check the reproducibility of the measurement. Each spectrum was normalized using the Labspec software.

CHAPTER 4

RESULTS AND DISCUSSION

In this chapter, SAMs of biological and organic molecules on gold and HOPG substrates have investigated with various techniques such as STM/STS, XPS, SERS, ellipsometry and contact angle goniometer. This chapter contains two parts based on investigation results of organic and biological molecules.

4.1. Investigation Results of Organic Molecules

In this part, we present the results of the SAMs of thiophenol, EPBB and BIBA molecules on Au(111) and HOPG.

4.1.1. Investigation Results of SAMs of Thiophenol

We investigated the molecular assembly of the thiophenol molecules on Au(111) surfaces by using STM and contact angle measurements. Thiopenol is an aromatic thiol with formula C_6H_6S. Also, the occurrence of delocalized π-electrons in the aromatic phenyl ring increases its electrical conductivity which makes thiophenol, aromatic thiols in general, a great candidate to study their SAMs kinetics. Aromatic thiol assemblies are interesting systems with delocalized π-electrons in the phenyl ring because of their electrical conductivity, rigidity and less molecular flexibility properties.

SAMs of thiophenol was prepared on Au(111) substrate by immersing Au(111) substrate in an ethanol solution for 12h. Figure 18(a) shows a topographic large-area STM image of thiophenol SAMs on Au(111) acquired in the constant-current mode. As shown in the Figure 18(a), it can be seen that gold terraces are covered with domain islands of well-ordered thiophenol molecules. Higher magnification STM images (Figure 18 (b-d)) of SAMs of thiophenol reveal that molecules are aligned into parallel stripes.

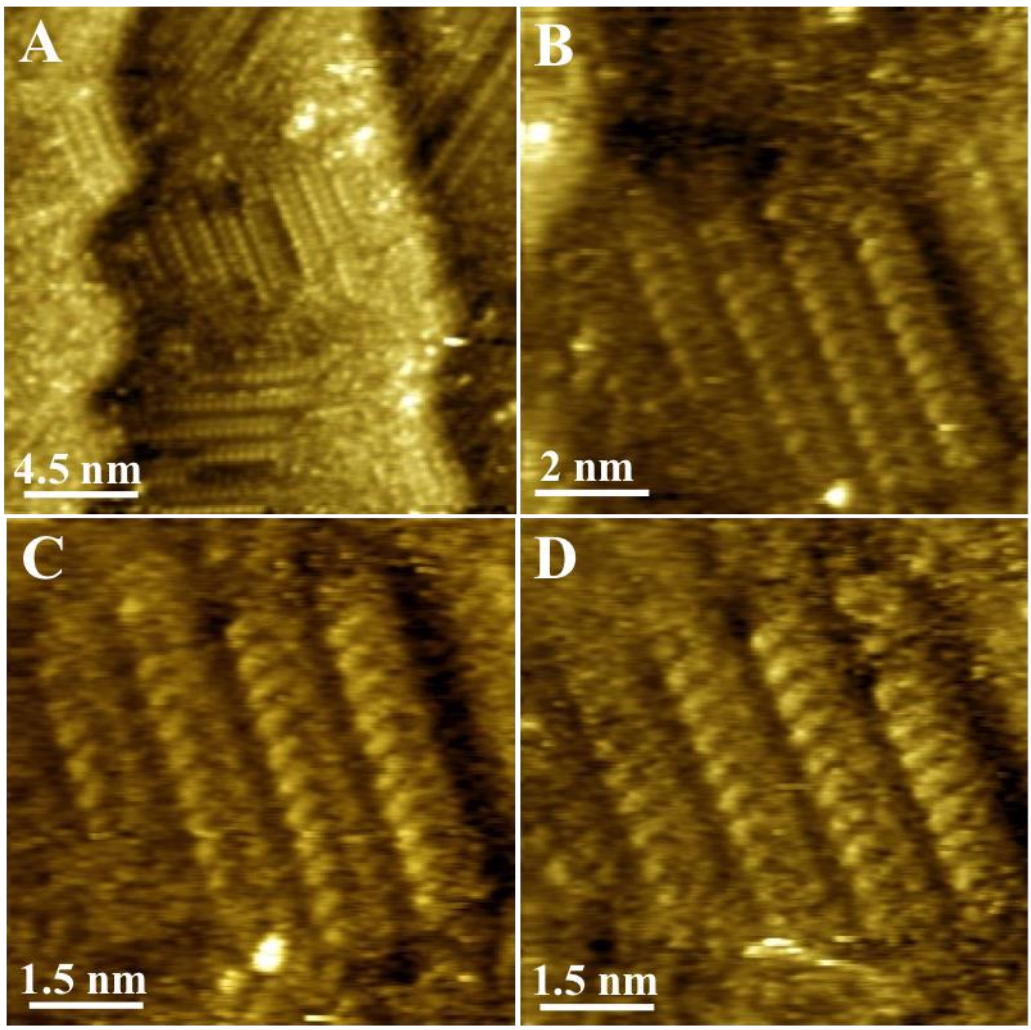

Figure 18. STM images of ordered assemblies of thiophenol. (a) Large area image, (b-d) Magnified view of the order region from image (a).

Contact angle measurements were performed with a sessile drop goniometer to determine the wettability of the surfaces. Firstly, a drop of water was placed on a bare Au(111) surface and after obtaining the angles from left and right side of the droplet, the average contact angle of the bare Au(111) surface was determined. It was found that the bare Au(111) surface has a contact angle of 64. Then, the same procedure was performed for thiophenol monolayers on gold and the average contact angle of thiophenol monolayer was found to be 76. The increase in the contact angles compared between the two surfaces shows that the Au(111) surface has a good coverage of thiophenol monolayer.

4.1.2. Invetigation Results of *(E)*-4-((4-(phenylethynyl)benzylidene) amino)benzenethiol (EPBB) SAMs

We investigated a newly designed Schiff base monolayer structures of EPBB molecules on Au(111) surface prepared via solution phase deposition. STM/STS and SERS experiments were used to probe the conformational change and switching behavior of the EPBB molecules with increasing tunneling current. Contact angle and ellipsometry measurements were used to get an understanding about thickness and wettability of the surface. XPS measurements were conducted to measure the chemical nature of EPBB molecules on Au(111) surface.

The structures of the self-assembled monolayer of EPBB molecular films on Au(111) were studied at atomic resolution using STM. A large area STM image is shown in Figure 19(a). This image contains many short-range islands with average sizes of 5 to 15 nm on Au(111). According to the images taken from 50 different areas of the same sample, approximately 80 percent of the surface was found to be occupied with these islands and the rest was generally covered by unorganized molecules. The organization of EPBB molecules as shown in Figure 19(b) demonstrated that the molecules were ordered in parallel rows and separated by 0.78 nm from each other. The domains yielded a nearly-oblique lattice with parameters a = 0.68±0.1 nm, b = 0.8±0.1 nm and α = 101° as determined from the STM image in Figure 19(b). The pattern in the organization of EPBB molecules on the Au(111) surface had the 2D triangular lattice symmetry of the Au(111) substrate. Atomic structure of an EPBB molecule changes, when *trans* isomers form a periodic SAM structure as the olecule changes, when 2D triange 0.78 nm from each other. The domains yielded a nearly-oblique lattice with parameent of the surface re.5 nm and then the substratentation. The STM experiments were conducted at 20 to 50 different regions of the sample. Thus *cis* formation took place in the entire sample when the sample was contacted with the STM tip. The structural transformation of the SAM while being scanned at high-current mode was attributed to the strong interaction of the STM-tip with the tail groups of the EPBB molecules on Au (111).

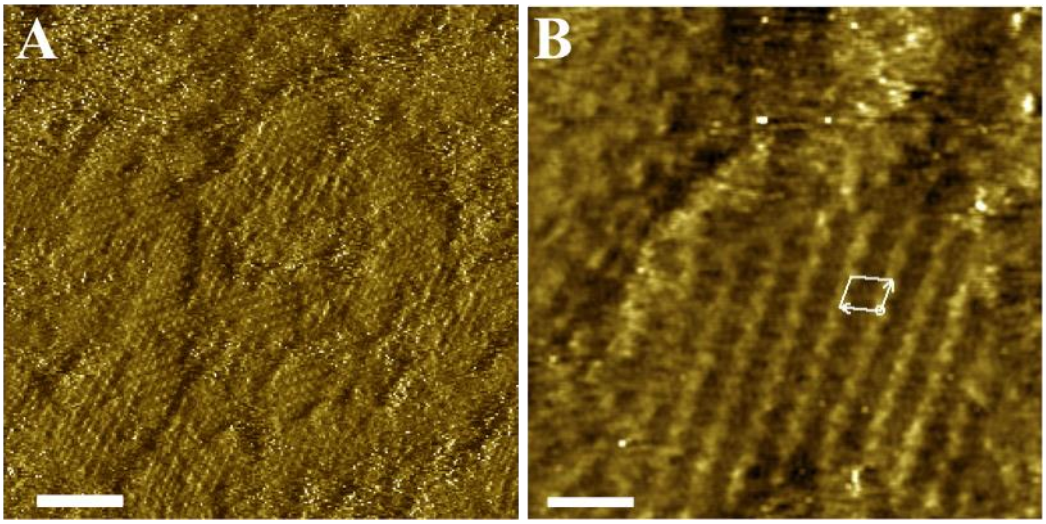

Figure 19. (a) STM image of a Au(111) surface after immersion in a chloroform solution of EPBB molecule (scale bar = 5.2 nm). (b) Magnified view of an ordered region from image A (scale bar = 1.5 nm).

In the next experiment on the switching mechanism, we applied a tunneling current to the domains in which the EPBB molecules on Au(111) were in the *trans* configuration as shown in Figures 20(a) and Figure 20(b). The close-up STM image shown in Figure 20(b) scanned with the same tunneling current (5 pA) and bias voltage (1 V) condition showed no changes on the morphology of the SAM. While increasing the tunneling current from 50 pA (Figure 20(c)), to 400 pA (Figure 20(d)), 600 pA (Figure 20(e)), 800 pA (Figure 20(f)), 1 nA (Figure 20(g)) and 1.2 nA (Figure 20(h)), we observed that the STM tip changed the EPBB monolayer significantly when the current was increased to 1.2 nA. From the comparison of STM images of EPBB monolayer, it can be seen that for lower tunnelling currents (Figures 20(c-f)) there are only slight changes in the rows of EPBB monolayer, but after the current reached 1-1.2 nA (Figures 20(g) and 20(h)). The morphology of the monolayer changed significantly. The reason of this can be explained as the molecular architecture tending to switch from *trans* to *cis* form. If we compare Figure 20(b) and Figure 20(h), it can be seen that all the molecules in the island changed their appearance and showed a lower height which was 1.2 nm as supported by ellipsometry measurements.

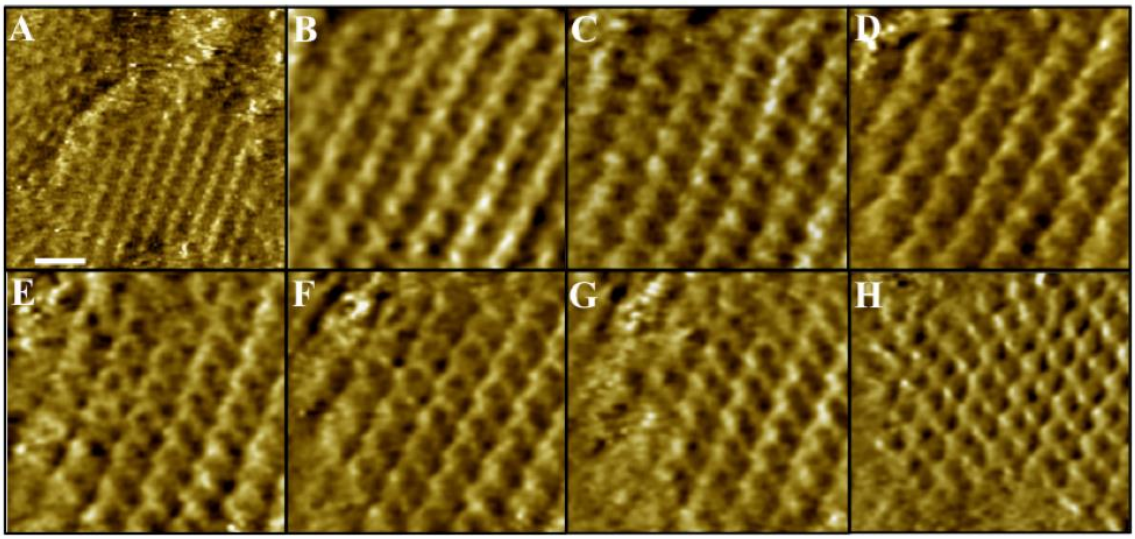

Figure 20. STM images of ordered assemblies of EPBB. The STM images were recorded under constant-current mode with tunneling current varying between 5 pA and 1.2 nA and a 1 V bias voltage. Images (a and b) 5 pA, (c) 50 pA, (d) 400 pA, (e) 600 pA, (f) 800 pA, (g) 1 nA and (h) 1.2 nA. Scale bar in (a) is 1.5 nm and for (b)-(h) it is 0.8 nm.

The image in Figure 20(h) indicated that the individual EPBB molecules in the monolayer were seen with a higher resolution, and the number of rows was doubled, due to the rotation and switching of the molecules induced by the effect of the tunneling current. It is clear that the ability to change the conformation by tuning the tunneling current allows us to control over the process. The transition was reversible only with external stimuli such as heating. A temperature of 55 °C turned the molecules from *cis* to *trans* form. The observed conformational change was unique because of two main reasons: (i) The EPBB molecule has *trans* and *cis* isomers and their energies are comparable to each other. Therefore, the transition that could not be observed for other molecules such as thiophenol took place for the assembly of special EPBB molecule. (ii) The attractive interaction between the upper most part of the EPBB molecule and the apex of the STM tip was essential. To sum up, the type of the molecule and the type of the intraction with STM tip were crucial for the mechanism of the transformation.

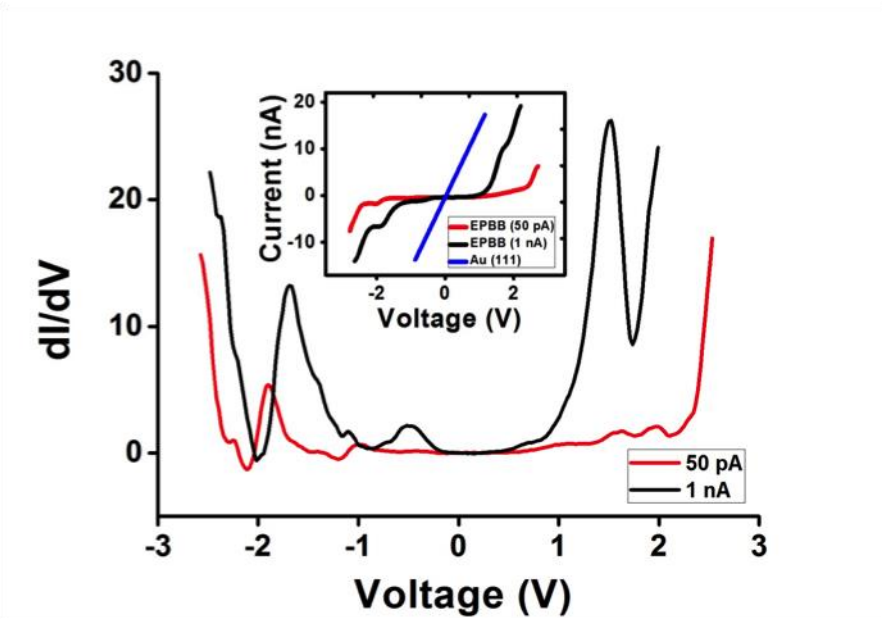

Figure 21. dI/dV characteristics of the EPBB molecule and of an Au substrate on mica. The inset shows current-voltage characteristics of the individual molecules of EPBB compared to that from a bare Au surface.

We investigated the electronic behavior of the EPBB SAMs by establishing their current-voltage dI/dV and I-V characteristics via scanning tunneling spectroscopy as shown in Figure 21. The STS measurements were performed at a fixed tip–sample distance with the feedback loop being switched off. Each I-V curve was averaged over at least 20 successive voltage sweeps. The time required for a complete spectroscopy measurement was below 0.1 second. The inset curves in Figure 21 show the I-V characteristics of bare Au (111), and EPBB monolayer at 50 pA (red) and 1.2 nA (black), respectively. Both of the I-V curves of EPBB showed semiconducting behavior, when compared with the bare Au (111) surface. From the dI/dV characteristic of EPBB, it can be seen that it has an average energy gap of 2.5 eV (50 pA) and 2.0 eV (1 nA), respectively. The SERS experiments were conducted to verify the transition of the EPBB molecules from *trans* to *cis* and its reversibility. Figure 22 shows the Raman spectrum of EPBB obtained with 785 nm laser. Figure 20(a) depicts the Raman spectra of *trans* form of EPBB molecules (black spectrum). After 365 nm UV irradition EPBB molecules switched into *cis* form (red spectrum). Upon the cease of UV irradiation and heating the sample upto 55°C, the EPBB molecules switched to initial *trans* form (blue spectrum). EPBB interacts with solid interfaces via thiol functional group forming metal–S–C bonds. The peak at 665 cm^{-1} corresponded to the C–S stretch. In the spectra

(Figure 22(b)), we mainly focused on a specific range between 1540 cm^{-1} and 1630 cm^{-1} to identify the *cis-trans* transition. The peaks at 1573 cm^{-1}, 1593 cm^{-1} and 1619 cm^{-1}, respectively, in the black spectrum arose from C–C stretch and C=C stretch of aromatic rings and C=N stretch of the molecule in trans form. After irradition by UV light, these peaks shifted to lower wavelengths indicating the formation of *cis* isomer (red spectrum) (Figure 22(c)). The strong C≡C stretch of ethynyl group was observed at 2216 cm^{-1} as shown in Figure 22(c) and this stretching mode also shifted due to rotation of the bond upon *cis* isomerisation. In the range between 700 cm^{-1} and 1300 cm^{-1}, these peaks showed C–C stretch, C–C, C–H bending and ring breathing modes (Figure 22(a)).

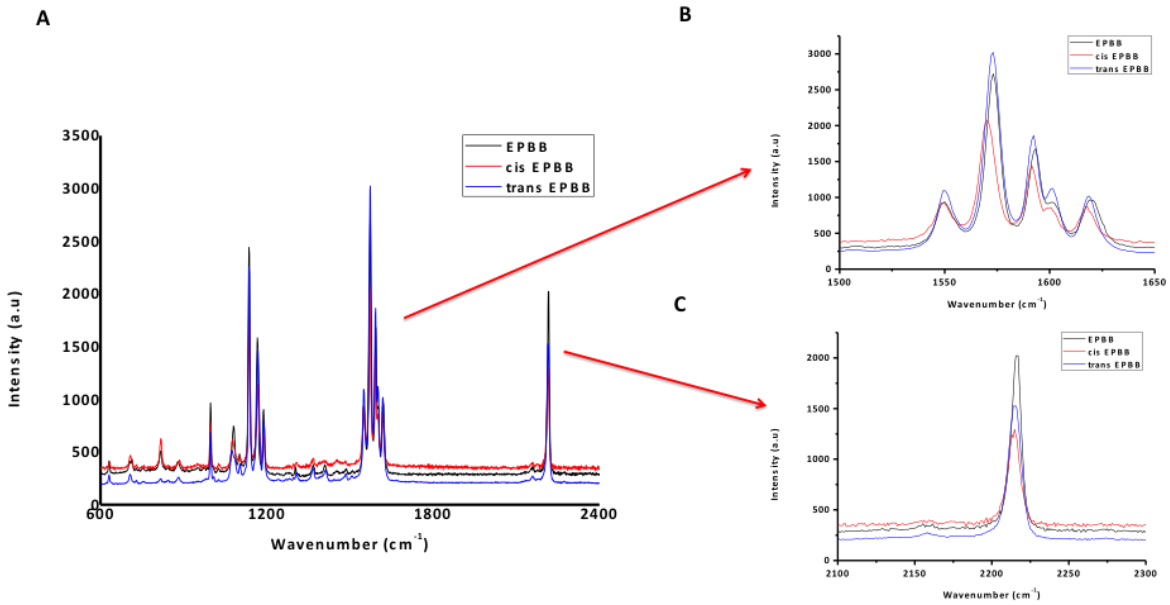

Figure 22. (a) SERS spectra of EPBB SAMs, Black spectra illustrate the EPBB molecules before UV irradiation or *trans* mode, Red spectra demonstrate the *cis* form of the SAMs after UV irradiation and Blue spectra indicate the *cis* to *trans* isomerization after heated to 55°C. (b) Enlarge spectrum of 1500-1650 cm^{-1}, (c) enlarge spectrum of 2200-2230 cm^{-1}.

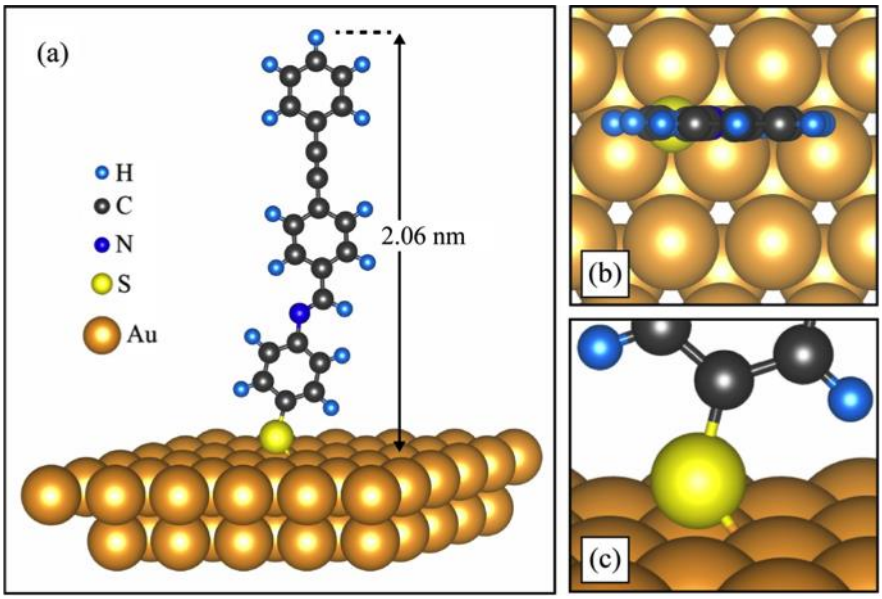

Figure 23. (a) Side view of optimized single EPBB molecule on Au (111) surface. (b) Top view and (c) tilted side view.

The thickness of the SAM of EPBB molecules on Au(111) was measured by using a Woollam spectroscopic ellipsometry (M-2000). A thickness of 2.12 ± 0.1 nm was obtained by using a Cauchy layer model for fitting the data set. Refractive index of the EPBB molecules determined as 1.44 via a refractometer and this data was used in the Cauchy layer model. The thickness measured by ellipsometry was in good agreement with theoretically calculated thickness (2.06 nm) of the EPBB molecules (Figure 23) assembled through S–Au bonding on the surface with a 30° angle. The measured thickness was slightly less than the thickness of 2.12 ± 0.1 nm for an EPBB monolayer in a perpendicular orientation relative to the surface, suggesting that the molecules are not perfectly perpendicular with respect to the gold surface. Indeed there may be some areas that are not monolayer. These areas of defects may be due to unorganized SAM that may appear from multilayer or Au (111) defects. However, the thickness measurement performed by ellipsometry showed that the sample was mainly composed of monolayer SAM. A thickness of 1.2 nm was obtained after *cis-trans* transition. Ellipsometry results were presented in ellipsometric angles (Ψ and Δ) vs wavelength graphs and can be seen in Figure 24 to show the change of monolayer thickness after *cis-trans* transition.

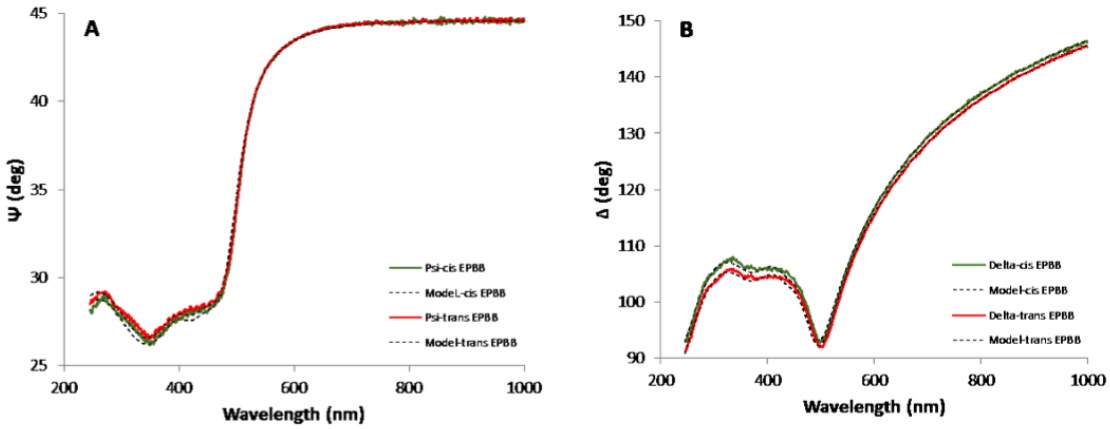

Figure 24. Spectroscopic Ellipsometric (SE) spectra for both *trans* and *cis*-EPBB SAM on gold with Cauchy model. Dashed lines: fitting model, green lines: *cis* EPBB and red lines: *trans* EPBB.

Water contact angles were measured on freshly prepared surfaces. An advancing angle of 70° was recorded for the EPBB molecules on the Au(111) surface, while an angle of 64° was recorded for the untreated gold substrate under the same experimental conditions.

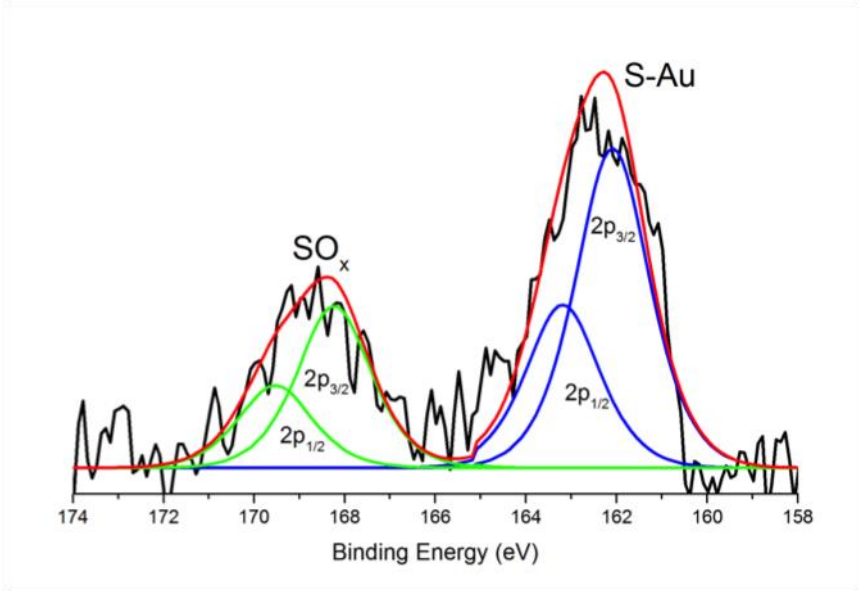

Figure 25. XPS spectra showing the S 2p region of the EPBB molecule.

A freshly prepared SAM of EPBB molecules was analyzed using XPS. The C 1s spectrum shown in Figure 26 was deconvoluted into 3 peaks; a major carbon species at 284.8 eV and two minor peaks at 287.5 eV and 290.7 eV. The ratio of intensities was 9.6:1.4:1.0, respectively. The major peak was assigned to the aromatic carbon in the molecule. The peak at 287.5 eV was carbonyl carbon while the peak at 290.7 eV was most likely due to O(CO)O type moieties from the impurities on the surface. The N1s region as can be seen in Figure 26 showed a broad peak, which could be deconvoluted into two peaks at 398.6 eV and 401.0 eV with 1.7 to 1.0 ratio. While the stronger peak at lower binding energy corresponded to the nitrogen atoms within the molecule, the weaker peak at higher binding energy suggested an oxidized nitrogen species. The sulfur spectrum shown in Figure 25 showed two 2p doublets at 161.8 eV ($2p_{3/2}$) and 167.9 eV ($2p_{3/2}$). The first doublet can be assigned to sulfur linking the molecule to the gold substrate, while the latter indicates the presence of oxidized sulfur species. The O 1s region as shown in Figure 26 showed a weak and broad peak at 531.7 eV. The presence of oxygen and oxidized nitrogen, sulfur and carbon species reveal a slight inclination towards oxidation. As can be seen in Figure 25, the intensity of the $2p_{3/2}$ peak at 167.9 eV for the oxidized sulfur (SO_x) species reaches about half the intensity of the thiol sulfur. This is an expected result as the oxidation of sulfur proceeds with a lower activation barrier compared to carbon. The oxidized carbon species, on the other hand, have only 10 percent of the aliphatic carbon intensity, at 287.5 eV and 290.5 eV for the carbonyl and carboxyl moieties, respectively.

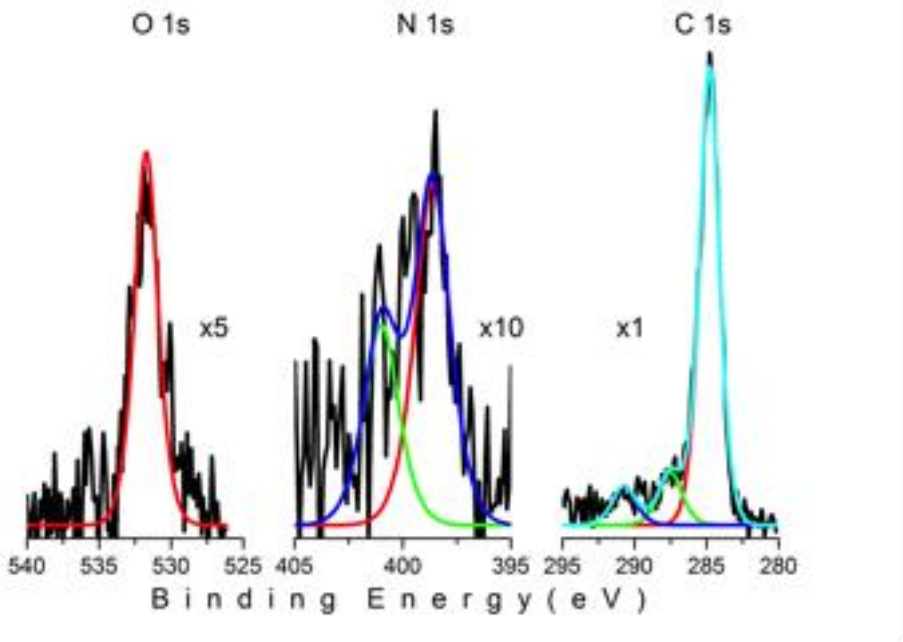

Figure 26. XPS spectra showing the O 1s, N 1s and C 1s regions of EPBB molecule.

4.1.3. Investigation Results of SAMs of 4-(4,7-Di(thiophen-2-yl)-*1H*-benzo[d]imidazol-2-yl)benzaldehyde (BIBA)

Here, we focus on surface morphology of BIBA monolayers on Au(111). BIBA SAMs on Au(111) were investigated by using STM/STS. For STM investigation, samples were prepared by immersing Au(111) substrate in a chloroform solution at room temperature overnight. STM images were acquired in ambient conditions with a bias voltage of 1 V and a tunneling current of 200 pA. BIBA molecules were chemisorbed on Au(111) surface via sulfur atoms. A large-area STM image of BIBA monolayer on Au(111) can be seen in Figure 27(a). It reveals step edges of Au(111) surface densely covered with ordered areas of BIBA. A close-up STM image of BIBA monolayer over a scan area of 85 nm x 85 nm can be seen in Figure 27(b) and it shows some vacancy islands that were formed on the surface alongside with the ordered BIBA monolayers on Au(111). Figure 27(c) and Figure 27(d) shows that the higher resolution STM images of BIBA monolayers are well-ordered in parallel strips.

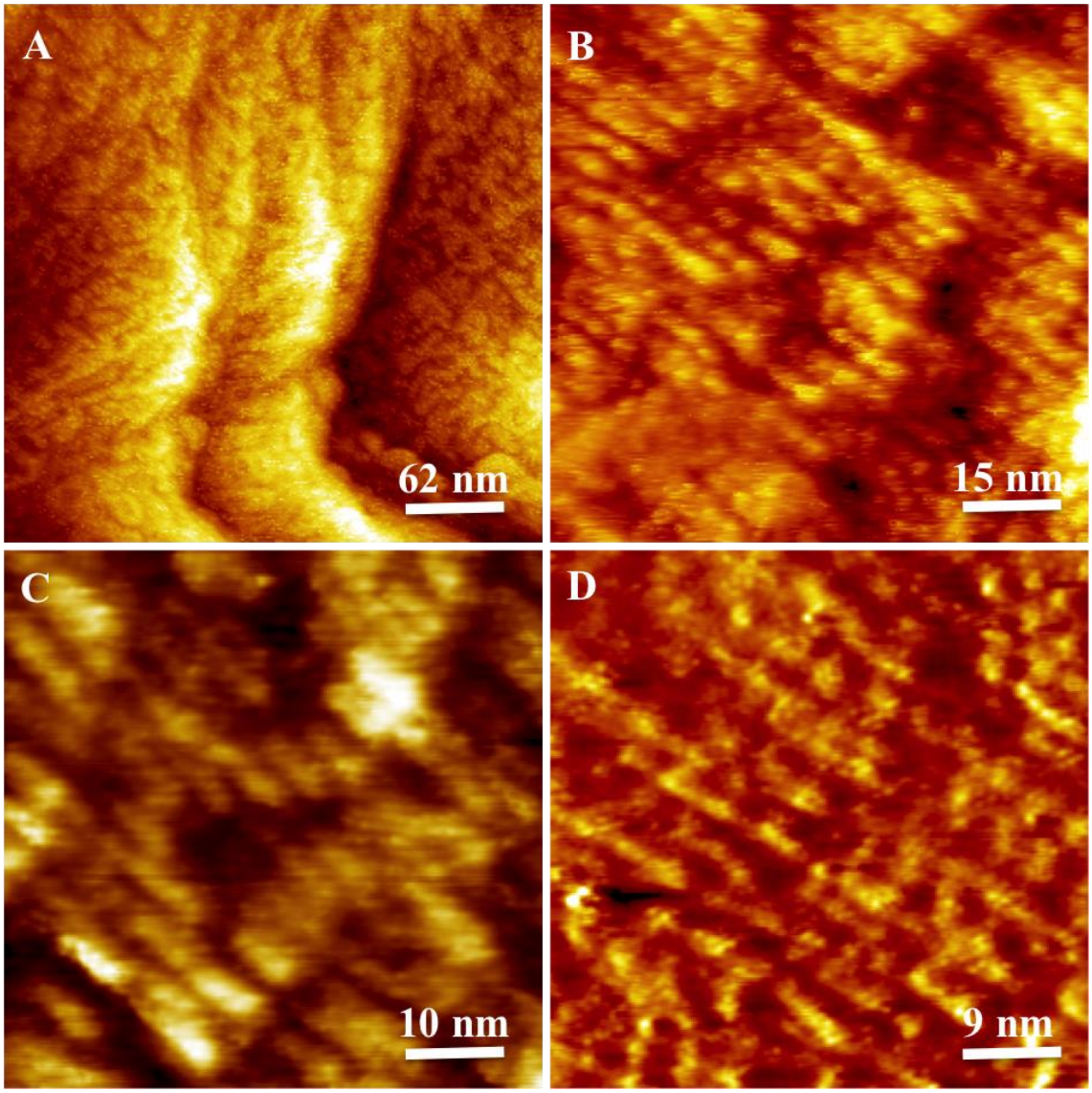

Figure 27. (a-d) STM images of BIBA assemblies on Au(111).

I-V curve of BIBA molecule on Au(111) was obtained by scanning tunneling spectroscopy experiments. STS study was performed with the feedback loop switched off. A bias voltage between – 3V and + 3V applied for a time of 0.1 s. Figure 28 shows the I-V characteristics of BIBA molecule on Au(111) with semiconductor behavior.

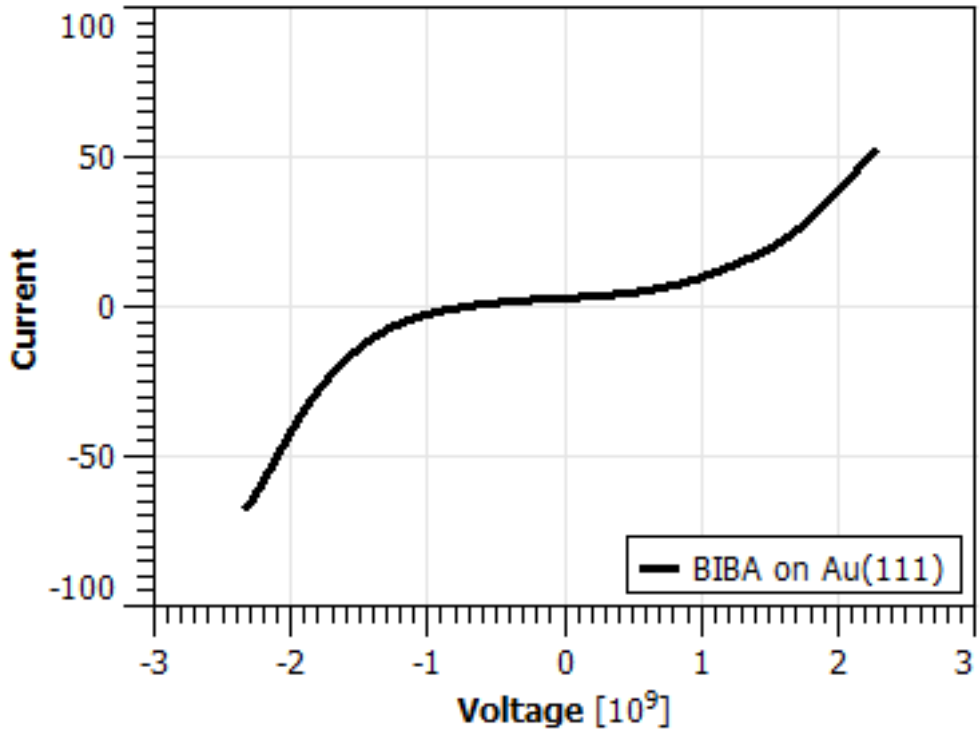

Figure 28. I-V curve of BIBA on Au(111)

Later, surface morphology of BIBA monolayer on HOPG surface was investigated by using STM. BIBA monolayer was prepared by depositing a drop of BIBA solution on HOPG surface and left to dry at room temperature. STM images of SAMs were acquired with a bias voltage of 400 mV and a tunneling current of 200 pA.

Figure 29(a) shows a STM image of BIBA SAM on HOPG surface with a scan area of 123 nm x 123 nm. It can be clearly seen that BIBA monolayer was densely packed on HOPG surface with different molecular orientations. Higher magnification of STM images of BIBA monolayer can be seen in Figure 29(b) and Figure 29(c). Line profile on the STM image of BIBA monolayer in Figure 29(c) indicates an inter-row spacing of 1.2 and an intra-row spacing of 1.8 nm.

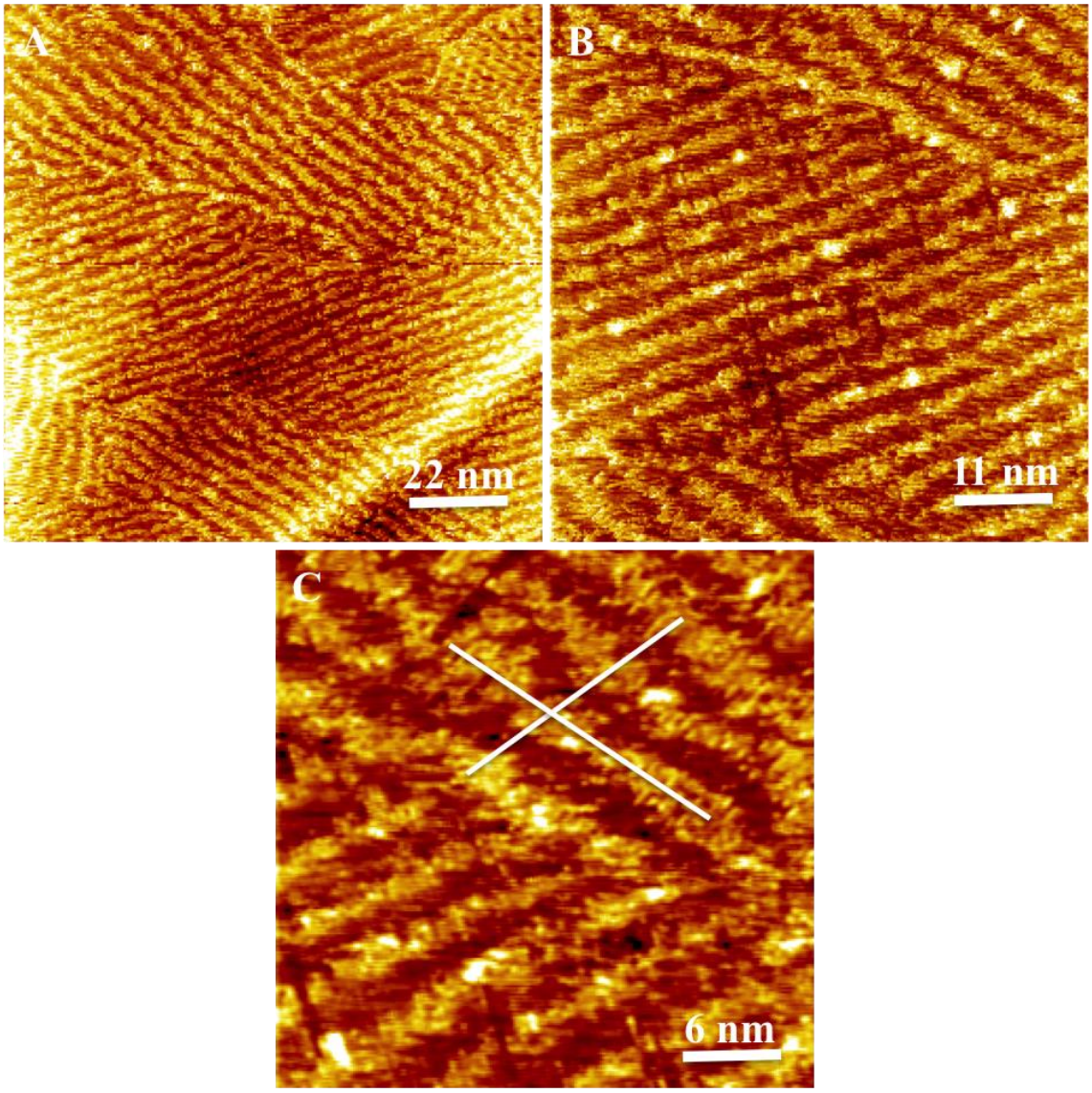

Figure 29. (a-c) STM images of BIBA on HOPG.

4.2. Investigation Results of Biological Molecules

Here, we show the investigation results of SAMs of biological molecules on Au(111) and HOPG surfaces.

4.2.1. Investigation Results of Mixed SAMs of Biotin-Streptavidin

We investigated the mixed SAMs of biotinylated disulfide (Biotin-HPDP) and thiophenol monolayers and the immobilization of streptavidin on biotin molecules on Au(111) surfaces by using STM. Moreover, we tried to understand the effects of molar ratio of mixed SAMs monolayers on streptavidin – biotin binding affinity. Firstly, we prepared mixed SAMs of biotin-HPDP and thiophenol on Au(111) by solution phase depositon method with a molar ratio of 1:9. Figure 30 shows STM images of mixed Biotin-HPDP and thiophenol SAMs on Au(111) surface scanned with a bias voltage of 1 V and a tunneling current of 200 pA. Gold terraces covered with mixed molecules can be seen in Figure 30(a) and 30(b). Higher magnification STM images of mixed Biotin-HPDP/thiophenol reveal small domains of organized thiophenol monolayer, as shown in Figure 30(c) and 30(d). Bright dots in Figure 30(c) indicate the Biotin-HPDP molecules on Au(111) surface.

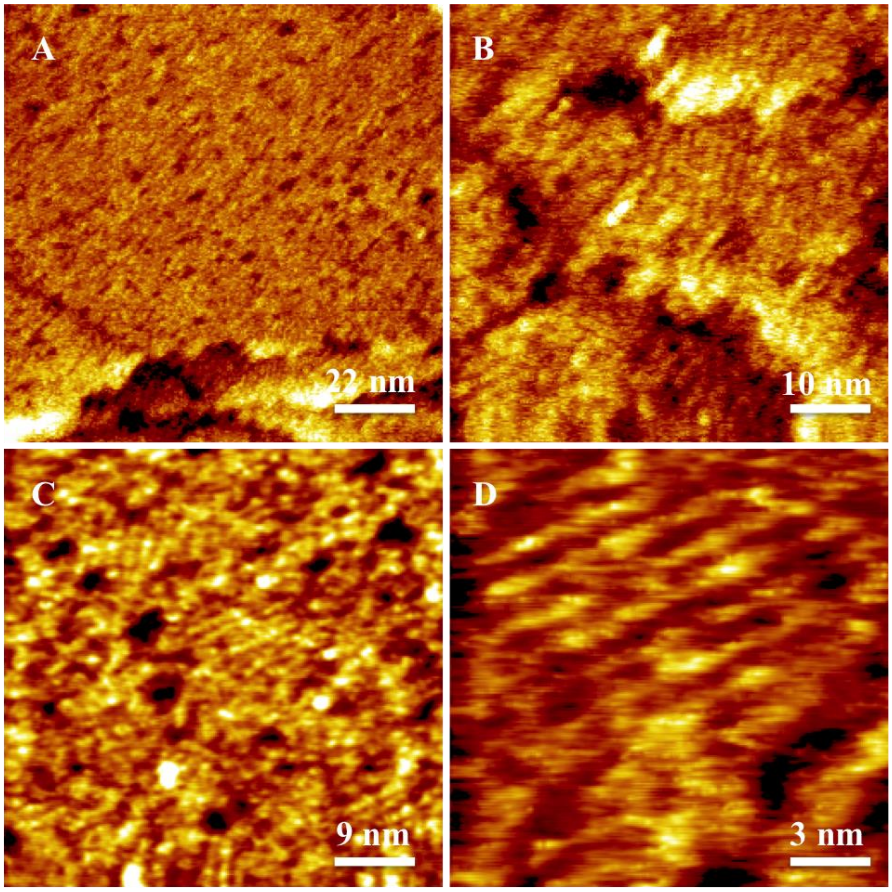

Figure 30. (a-d) STM images of 1:9 Mixed SAMs prior to the immobilization of streptavidin.

Next, we immobilized the streptavidin molecules to the mixed SAM on Au(111) surface by immersing into a solution of streptavidin in PBS buffer. After the immobilization of streptavidin molecules to the mixed SAM on Au(111) surface, STM experiments were repeated. Figure 31 shows the STM images of Au(111) surface after streptavidin binding to the mixed SAM. The big bright dots indicate the streptavidin molecules binding to Biotin-HPDP. Figure 31(c) shows a higher magnification STM image of streptavidin molecules on mixed SAM surface. Apparent diameter of streptavidin molecule is estimated to be 4 nm from the line profile on image in Figure 32, the height of the bright spots is 6 nm which is in good agreement with the size of a free streptavidin molecule. A single streptavidin molecule can be seen clearly in higher resolution in Figure 31(d).

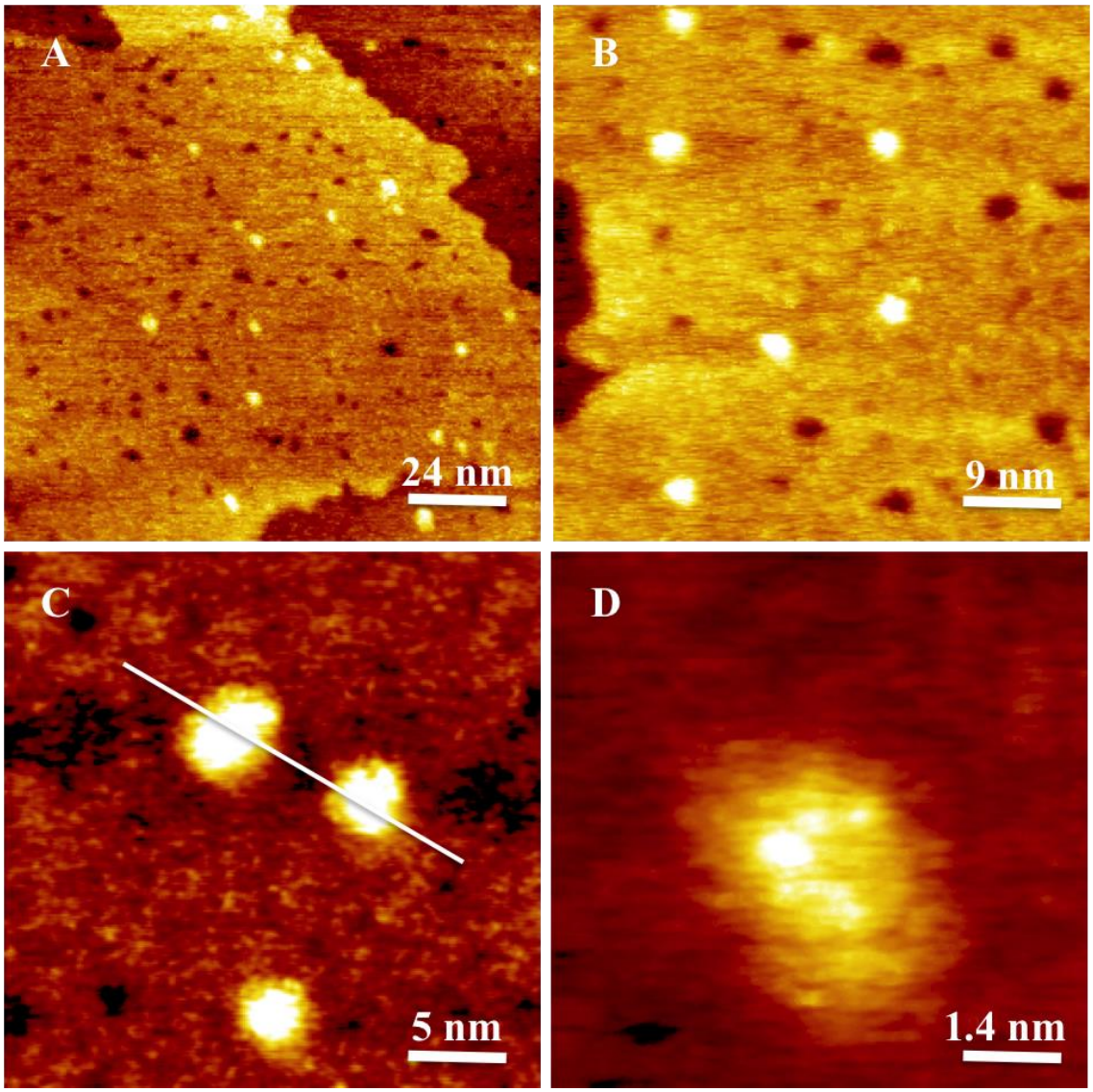

Figure 31. (a-d) STM images of 1:9 Mixed SAMs after the immobilization of streptavidin.

Figure 32. Line profile of streptavidin.

To determine the optimal mixing ratio of the SAMs for better coverage of streptavidin molecules, we prepared two more mixed biotin-HPDP/thiophenol SAMs with a molar ratio of 5:5 and 7:3, respectively. Figure 33 shows STM images of mixed SAMs prepared with a molar ratio of 5:5 after the immobilization of streptavidin. Figure 33(a) shows a large area STM image of step edges of gold terraces covered with mixed SAM and no evidence of streptavidin molecules. Higher magnification STM images (Figure 33(c) and 33(d)) shows well-ordered mixed SAM aligned into rows.

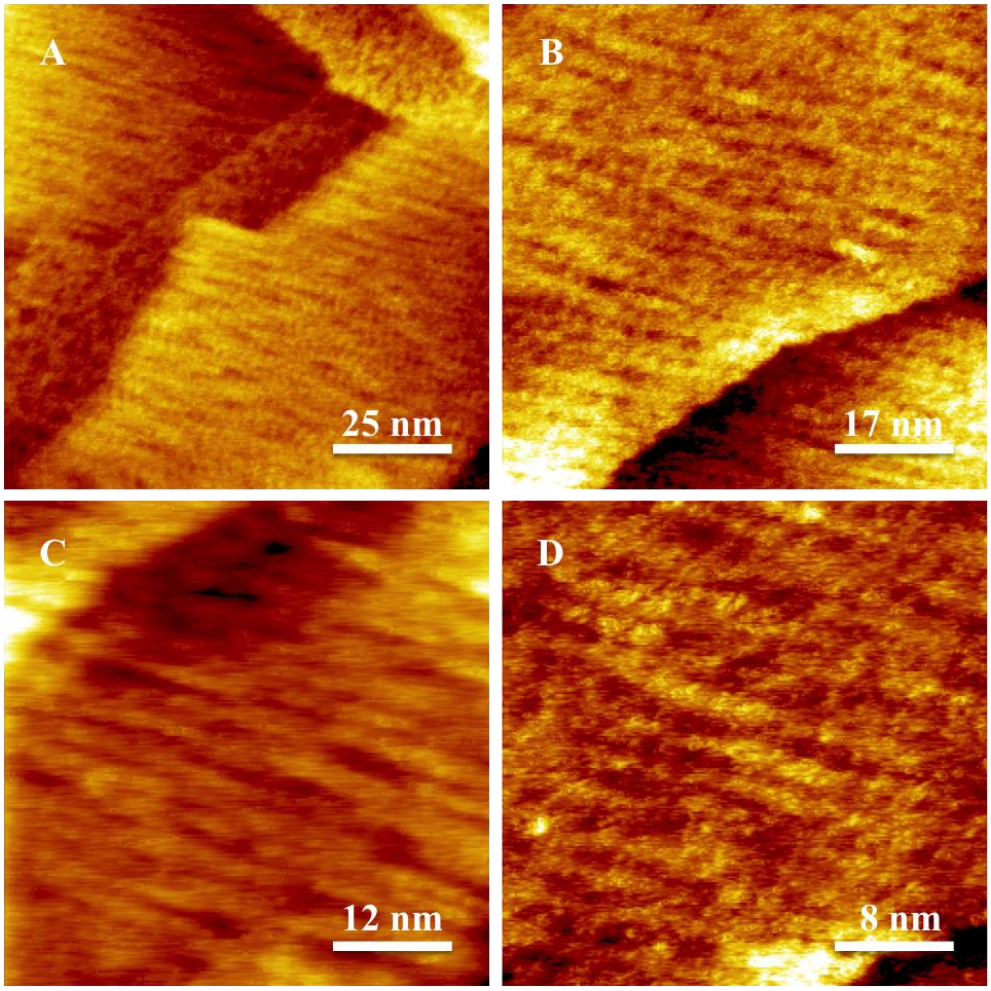

Figure 33. (a-d) STM images of 5:5 Mixed SAMs after the immobilization of streptavidin.

Figure 34 shows STM images of mixed SAMs prepared with a molar ratio of 7:3 after the immobilization of streptavidin. If we compare Figure 30(a) and Figure 34(a), it can be seen that increase in the molar ratio of Biotin-HPDP resulted in a change of surface morphology of SAMs. Surface coverage of mixed SAM of Biotin-HPDP/thiophenol with a molar ratio of 1:9 is slightly different than the one with molar ratio of 7:3. From STM image (Figure 34(a)) of mixed SAM, there is no evidence of streptavidin molecules on the surface. The reason for this can be explained as a result of steric hindrance due to the close packing of biotin molecules on Au(111) surface. We can clearly say that the best optimal molar ratio of mixed SAMs for streptavidin immobilization is 1:9 as reported in the previous studies [59].

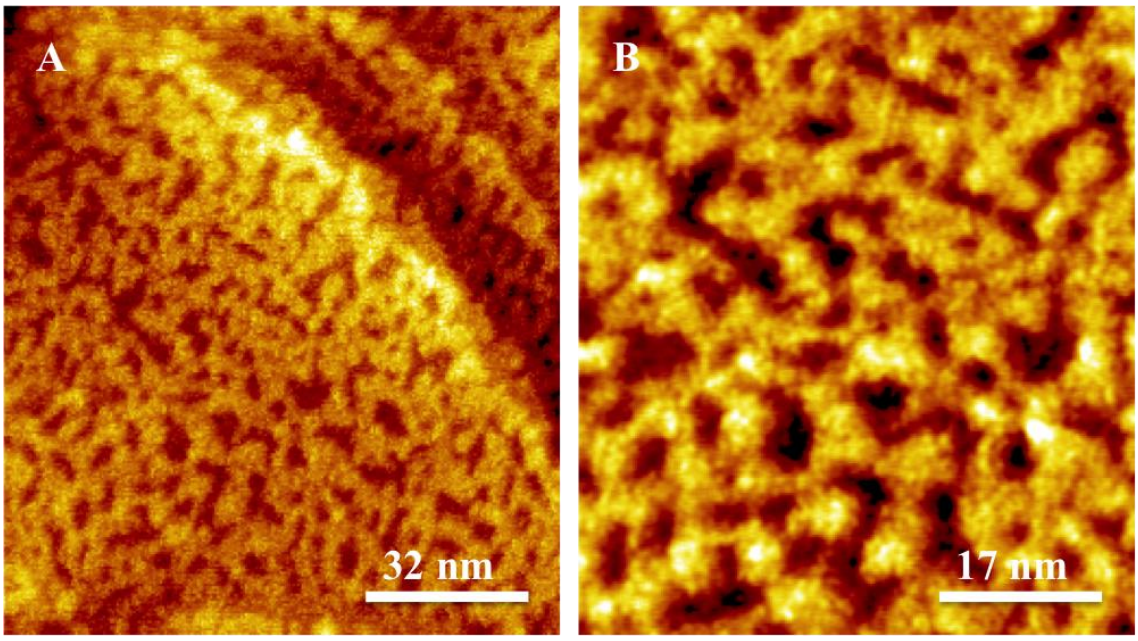

Figure 34. STM images of 7:3 Mixed SAMs after the immobilization of streptavidin.

4.2.2. Investigation Results of SAMs of Graphite-Binding Peptide (GrBP5)

We investigated the assembly characteristics of GrBP5 on HOPG surface by using STM to understand the surface morphology of wild-type graphite-binding peptide assemblies. Molecular assembly of GrBP5 monolayers, prepared with a peptide solution of 1 μM in distilled water for 1 h on HOPG surface. The sample was immediately investigated with STM. Figure 35(a) shows the large magnification STM image of GrBP5 monolayer with a scan area of 120 nm x 120 nm. It reveals that GrBP5 was well organized with different assembly orientations over HOPG surface. The higher magnification STM image of peptide assembly in Figure 35(b) shows highly ordered monolayers of peptide molecules aligned into rows. High-resolution STM images of peptide assemblies are shown in Figure 35(c) and 35(d).

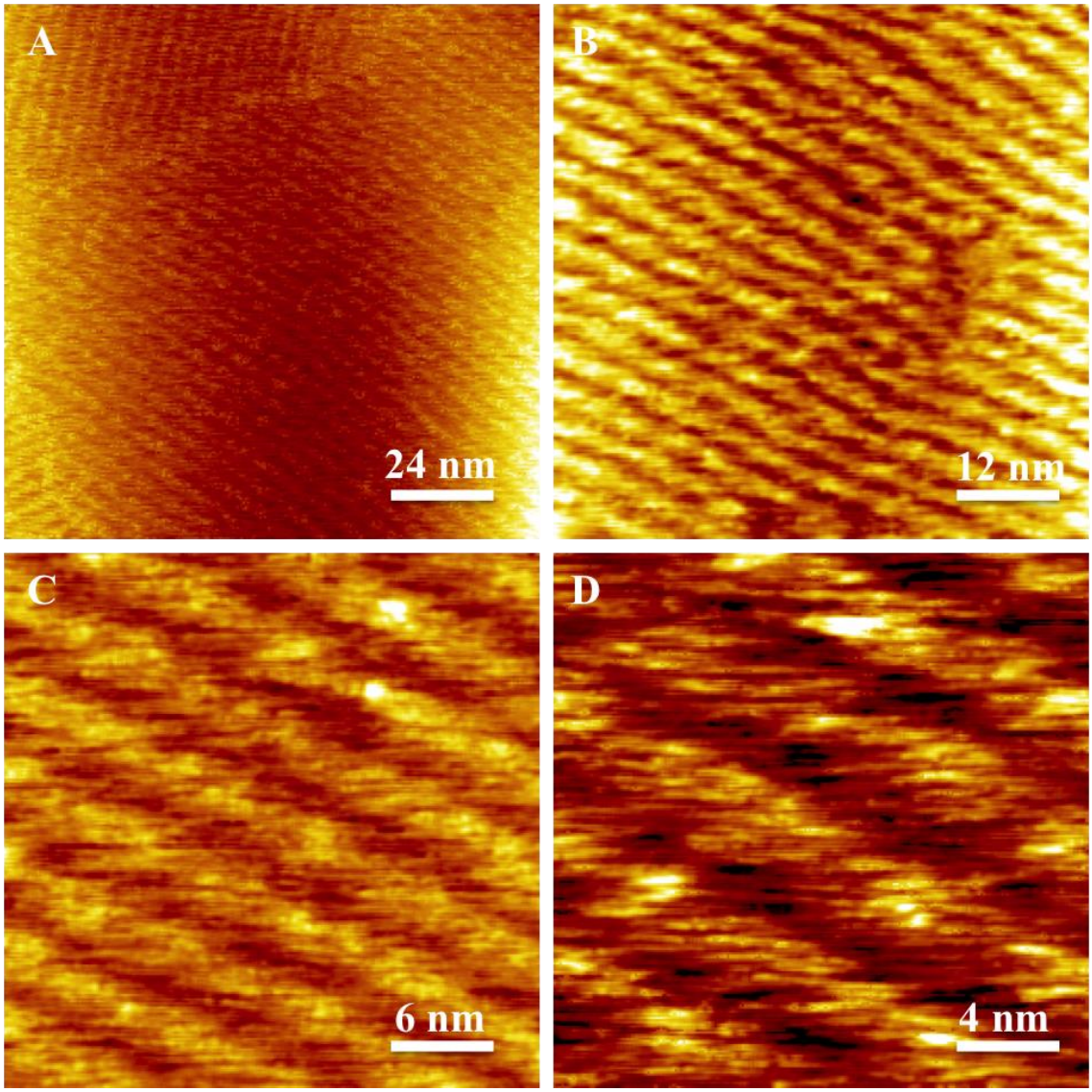

Figure 35. (a-d) STM images of GrBP5 on HOPG.

I-V curve of GrBP5 monolayer on HOPG was obtained by scanning tunneling spectroscopy experiments. STS study was performed with the feedback loop switched off. A bias voltage between – 2,5 V and + 2,5 V applied for a time of 1 s. Figure 36 shows the I-V characteristics of BIBA monolayer on Au(111) and it reveals that I-V curve of GrBP5 monolayer exhibits semiconductor behavior.

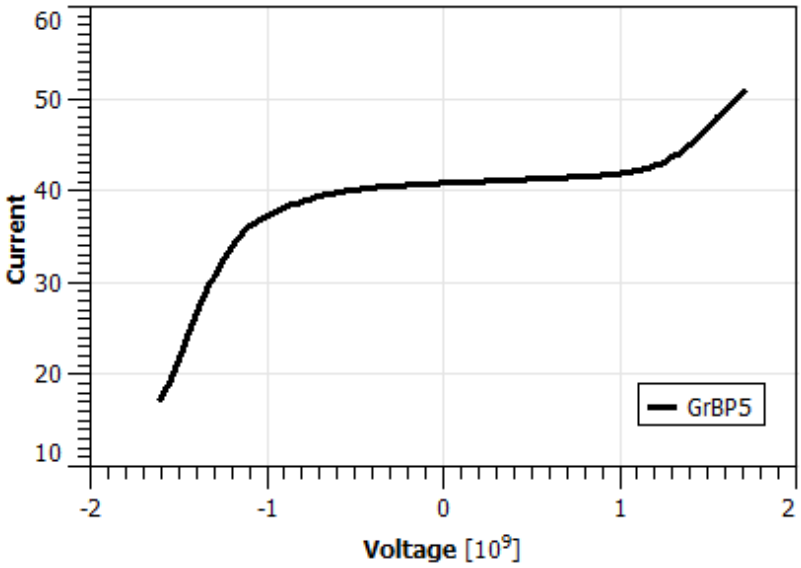

Figure 36. I-V curve of GrBP5.

CHAPTER 5

CONCLUSION

This thesis reveals the investigation of organic and biological molecular assemblies deposited on gold and graphite surfaces.

Thiophenol SAMs were investigated with STM and contact angle measurements and it was found that thiophenol monolayers were aligned into striped phase.

The exposure of Au(111) surfaces to EPBB in basic chloroform or dichloromethane solution resulted in the formation of a short-range order and long term stable monolayer. STM data showed that a chemisorption process took place and that molecular-sized features were evident on the surface. The binding of EPBB onto gold through S-Au bond was determined by XPS. The SERS spectra clearly show the transition of EPBB molecules from *trans* to *cis* and its reversibility.

BIBA SAMs were prepared both on Au(111) and HOPG surfaces. STM data showed well-defined ordered monolayer structure.

Mixed SAMs of biotin/thiophenol were prepared on Au(111) with different molar ratios to see the effects of these different molar ratios to the immobilization of streptavidin on mixed SAMs of biotin on Au(111). It was found that molar ratio of 1:9 is the best for the streptavidin immobilization.

Graphite-binding peptide assemblies on HOPG surface were investigated by STM and STS studies. STM data showed the ordered peptide assemblies on HOPG surface and STS data showed semi-conductor behavior of peptide assemblies.

REFERENCES

1. Bigelow, W., D. Pickett, and W. Zisman, *Oleophobic monolayers: I. Films adsorbed from solution in non-polar liquids.* Journal of Colloid Science, 1946. **1**(6): p. 513-538.

2. Sagiv, J., *Organized monolayers by adsorption. 1. Formation and structure of oleophobic mixed monolayers on solid surfaces.* Journal of the American Chemical Society, 1980. **102**(1): p. 92-98.

3. Netzer, L. and J. Sagiv, *A new approach to construction of artificial monolayer assemblies.* Journal of the American Chemical Society, 1983. **105**(3): p. 674-676.

4. Nuzzo, R.G. and D.L. Allara, *Adsorption of bifunctional organic disulfides on gold surfaces.* Journal of the American Chemical Society, 1983. **105**(13): p. 4481-4483.

5. Hähner, G., R. Hofer, and I. Klingenfuss, *Order and orientation in self-assembled long chain alkanephosphate monolayers adsorbed on metal oxide surfaces.* Langmuir, 2001. **17**(22): p. 7047-7052.

6. Helmy, R. and A.Y. Fadeev, *Self-assembled monolayers supported on TiO2: comparison of C18H37SiX3 (X= H, Cl, OCH3), C18H37Si (CH3) 2Cl, and C18H37PO (OH) 2.* Langmuir, 2002. **18**(23): p. 8924-8928.

7. Ogawa, H., T. Chihara, and K. Taya, *Selective monomethyl esterification of dicarboxylic acids by use of monocarboxylate chemisorption on alumina.* Journal of the American Chemical Society, 1985. **107**(5): p. 1365-1369.

8. Schlotter, N., et al., *Formation and structure of a spontaneously adsorbed monolayer of arachidic on silver.* Chemical physics letters, 1986. **132**(1): p. 93-98.

9. Hickman, J.J., et al., *Toward orthogonal self-assembly of redox active molecules on platinum and gold: selective reaction of disulfide with gold and isocyanide with platinum.* Langmuir, 1992. **8**(2): p. 357-359.

10. Schwartz, D.K., *Mechanisms and kinetics of self-assembled monolayer formation.* Annual Review of Physical Chemistry, 2001. **52**(1): p. 107-137.

11. Ulman, A., *An Introduction to Ultrathin Organic Films: From Langmuir--Blodgett to Self--Assembly*. 2013: Academic press.

12. Schreiber, F., *Self-assembled monolayers: from 'simple'model systems to biofunctionalized interfaces.* Journal of Physics: Condensed Matter, 2004. **16**(28): p. R881.

13. Vericat, C., et al., *Surface characterization of sulfur and alkanethiol self-assembled monolayers on Au (111).* Journal of Physics: Condensed Matter, 2006. **18**(48): p. R867.

14. Azzam, R. and N. Bashara, *Ellipsometry and polarized light, 1987.* Amsterdam, North-Holland., 1981.

15. Förch, R., H. Schönherr, and A.T.A. Jenkins, *Surface design: Applications in bioscience and nanotechnology*. 2009: John Wiley & Sons.

16. Bain, C.D., et al., *Formation of monolayer films by the spontaneous assembly of organic thiols from solution onto gold.* Journal of the American Chemical Society, 1989. **111**(1): p. 321-335.

17. Arnold, R., et al., *Preparation, modification, and crystallinity of aliphatic and aromatic carboxylic acid terminated self-assembled monolayers.* Langmuir, 2002. **18**(10): p. 3980-3992.

18. Wang, H., et al., *Improved method for the preparation of carboxylic acid and amine terminated self-assembled monolayers of alkanethiolates.* Langmuir, 2005. **21**(7): p. 2633-2636.

19. Xiao, X., et al., *Thermal annealing effect of alkanethiol monolayers on Au (111) in air.* Surface science, 2001. **472**(1): p. 41-50.

20. Huang, C., et al., *Polymer blend lithography: A versatile method to fabricate nanopatterned self-assembled monolayers.* Beilstein journal of nanotechnology, 2012. **3**(1): p. 620-628.

21. Hähner, G., et al., *Investigation of intermediate steps in the self-assembly of n-alkanethiols on gold surfaces by soft X-ray spectroscopy.* Langmuir, 1993. **9**(8): p. 1955-1958.

22. Poirier, G. and E. Pylant, *The self-assembly mechanism of alkanethiols on Au (111).* Science, 1996. **272**(5265): p. 1145-1148.

23. Belton, G., *Langmuir adsorption, the Gibbs adsorption isotherm, and interracial kinetics in liquid metal systems.* Metallurgical Transactions B, 1976. **7**(1): p. 35-42.

24. Yamada, R. and K. Uosaki, *In situ scanning tunneling microscopy observation of the self-assembly process of alkanethiols on gold (111) in solution.* Langmuir, 1998. **14**(4): p. 855-861.

25. Xu, S., et al., *In situ studies of thiol self-assembly on gold from solution using atomic force microscopy.* Journal of Chemical Physics, 1998. **108**(12).

26. Schreiber, F., et al., *Adsorption mechanisms, structures, and growth regimes of an archetypal self-assembling system: Decanethiol on Au (111).* Physical Review B, 1998. **57**(19): p. 12476.

27. Ulman, A., *Formation and Structure of Self-Assembled Monolayers.* Chem. Rev, 1996. **96**: p. 1533-1554.

28. Whitesides, G.M. and P.E. Laibinis, *Wet chemical approaches to the characterization of organic surfaces: self-assembled monolayers, wetting, and the physical-organic chemistry of the solid-liquid interface.* Langmuir, 1990. **6**(1): p. 87-96.

29. Love, J.C., et al., *Self-assembled monolayers of thiolates on metals as a form of nanotechnology.* Chemical reviews, 2005. **105**(4): p. 1103-1170.

30. Vericat, C., et al., *Self-assembled monolayers of thiols and dithiols on gold: new challenges for a well-known system.* Chemical Society Reviews, 2010. **39**(5): p. 1805-1834.

31. Scherer, J., et al., *Corrosion of alkanethiol-covered Cu (100) surfaces in hydrochloric acid solution studied by in-situ scanning tunneling microscopy.* Langmuir, 1997. **13**(26): p. 7045-7051.

32. Homola, J., *Surface plasmon resonance sensors for detection of chemical and biological species.* Chemical reviews, 2008. **108**(2): p. 462-493.

33. De Boer, B., et al., *Synthesis and characterization of conjugated mono-and dithiol oligomers and characterization of their self-assembled monolayers.* Langmuir, 2003. **19**(10): p. 4272-4284.

34. Lee, A.Y., A. Ulman, and A.S. Myerson, *Crystallization of amino acids on self-assembled monolayers of rigid thiols on gold.* Langmuir, 2002. **18**(15): p. 5886-5898.

35. Bain, C.D., J. Evall, and G.M. Whitesides, *Formation of monolayers by the coadsorption of thiols on gold: variation in the head group, tail group, and solvent.* Journal of the American Chemical Society, 1989. **111**(18): p. 7155-7164.

36. Pale-Grosdemange, C., et al., *Formation of self-assembled monolayers by chemisorption of derivatives of oligo (ethylene glycol) of structure HS (CH2) 11 (OCH2CH2) mOH on gold.* Journal of the American Chemical Society, 1991. **113**(1): p. 12-20.

37. Nelson, K.E., et al., *Surface characterization of mixed self-assembled monolayers designed for streptavidin immobilization.* Langmuir, 2001. **17**(9): p. 2807-2816.

38. Young, T., *An essay on the cohesion of fluids.* Philosophical Transactions of the Royal Society of London, 1805. **95**: p. 65-87.

39. Miller, J.D., et al., *Effect of roughness as determined by atomic force microscopy on the wetting properties of PTFE thin films.* Polymer Engineering & Science, 1996. **36**(14): p. 1849-1855.

40. Proctor, A. and P.M. Sherwood, *Data analysis techniques in x-ray photoelectron spectroscopy.* Analytical Chemistry, 1982. **54**(1): p. 13-19.

41. Siegbahn, K. and K. Edvarson, *β-ray spectroscopy in the precision range of 1: 105.* Nuclear Physics, 1956. **1**(8): p. 137-159.

42. Hertz, H., *Ueber einen Einfluss des ultravioletten Lichtes auf die electrische Entladung.* Annalen der Physik, 1887. **267**(8): p. 983-1000.

43. Einstein, A., *Über einen die Erzeugung und Verwandlung des Lichtes betreffenden heuristischen Gesichtspunkt.* Annalen der Physik, 1905. **322**(6): p. 132-148.

44. Van der Heide, P., *X-ray photoelectron spectroscopy: an introduction to principles and practices*. 2011: John Wiley & Sons.

45. Weimer, J.J., *X–Ray Photoelectron Spectroscopy.* Characterization of Materials, 2002.

46. Hofmann, S., D. Briggs, and M. Seah, *Practical Surface Analysis, Volume 1 Auger and X-ray Photoelectron Spectroscopy.* edd by D. Briggs and MP Seah (John Wiley & Sons, Chichester, 1990) p, 1990. **145**.

47. Lindau, I. and W. Spicer, *The probing depth in photoemission and Auger-electron spectroscopy.* Journal of Electron Spectroscopy and Related Phenomena, 1974. **3**(5): p. 409-413.

48. Striebel, C., A. Brecht, and G. Gauglitz, *Characterization of biomembranes by spectral ellipsometry, surface plasmon resonance and interferometry with regard to biosensor application.* Biosensors and Bioelectronics, 1994. **9**(2): p. 139-146.

49. Tompkins, H.G. and W.A. McGahan, *Spectroscopic ellipsometry and reflectometry: a user's guide*. 1999: Wiley.

50. Forouhi, A. and I. Bloomer, *Optical dispersion relations for amorphous semiconductors and amorphous dielectrics.* Physical review B, 1986. **34**(10): p. 7018.

51. Binnig, G., et al., *Tunneling through a controllable vacuum gap.* Applied Physics Letters, 1982. **40**(2): p. 178-180.

52. Bhushan, B., *Springer handbook of nanotechnology. 2004.* Springer-Verlag: Heidelbert. **99**: p. 145.

53. Fleischmann, M., P.J. Hendra, and A. McQuillan, *Raman spectra of pyridine adsorbed at a silver electrode.* Chemical Physics Letters, 1974. **26**(2): p. 163-166.

54. Jeanmaire, D.L. and R.P. Van Duyne, *Surface Raman spectroelectrochemistry: Part I. Heterocyclic, aromatic, and aliphatic amines adsorbed on the anodized*

silver electrode. Journal of Electroanalytical Chemistry and Interfacial Electrochemistry, 1977. **84**(1): p. 1-20.

55. Albrecht, M.G. and J.A. Creighton, *Anomalously intense Raman spectra of pyridine at a silver electrode.* Journal of the American Chemical Society, 1977. **99**(15): p. 5215-5217.

56. Natan, M.J., *Concluding remarks surface enhanced Raman scattering.* Faraday discussions, 2006. **132**: p. 321-328.

57. Kneipp, K., et al., *Approach to single molecule detection using surface-enhanced resonance Raman scattering (SERRS): A study using Rhodamine 6G on colloidal silver.* applied spectroscopy, 1995. **49**(6): p. 780-784.

58. Kneipp, K., et al., *Single molecule detection using surface-enhanced Raman scattering (SERS).* Physical review letters, 1997. **78**(9): p. 1667.

59. Zareie, H.M., et al., *Temperature-responsive self-assembled monolayers of oligo (ethylene glycol): control of biomolecular recognition.* Acs Nano, 2008. **2**(4): p. 757-765.